Phosphomonoesterase and phosphodiesterase activities in the Eastern Mediterranean in two contrasted seasonal situations

France Van Wambeke[1*], Pascal Conan[2,3], Mireille Pujo-Pay[2], Vincent Taillandier[4], Olivier Crispi[2], Alexandra Pavlidou[5], Morgane Didry[1], Christophe Salmeron[3], Elvira Pulido-Villena[1]

[1]Aix-Marseille Université, Université de Toulon, CNRS, IRD, Mediterranean Institute of Oceanography (MIO), Marseille, France

[2] Sorbonne Université, CNRS – UMR7621, Laboratoire d'Océanographie Microbienne (LOMIC), Observatoire Océanologique, 66650, Banyuls/mer, France

[3] Sorbonne Université, CNRS OSU STAMAR - UAR2017, 4 Place Jussieu, 75252 Paris cedex 05, France

[4] Sorbonne Université, CNRS, Laboratoire d'Océanographie de Villefranche (LOV), Villefranche-sur-Mer, France

[5] Hellenic Centre for Marine Research (HCMR), Institute of Oceanography, 46.7 km Athens-Sounio Av., Anavyssos 19013, Greece

Correspondence to: France Van Wambeke (france.van-wambeke@mio.osupytheas.fr)

Abstract. Dissolved organic phosphorus hydrolysis by marine planktonic microorganisms is a key process in the P cycle, particularly in P-depleted, oligotrophic environments. The present study assessed spatio-temporal variations of phosphomonoesterase (PME) and phosphodiesterase (PDE) activities using concentration kinetics in the eastern Mediterranean Sea during 2 contrasted situations: the end of winter (including a small bloom period), and autumn. The distribution and regulation of the maximum hydrolysis rates (Vm) and half-saturation constants (Km) of both ectoenzymes were assessed in relation to the vertical structure of the epipelagic layers. PME reached their maximum activities (Vm) after 1 µM MUF-P addition whereas, for PDE, it was necessary to add up to 50 µM bis-MUF-P to reach saturation state. On average, the Km of PDE was 33 ± 25- times higher than that of the PME. Vm of PME and Vm of PDE were linearly correlated. Conversely to the Km values, Vm were on the same order of magnitude for both ectoenzymes, their ratio (Vm PME:Vm PDE) ranging between 0.2 and 6.3). Dissolved organic phosphorus (DOP) and the phosphomonoesterease hydrolysable fraction of DOP

explained mostly no variability of Vm PME nor Vm PDE. On the contrary, Vm of both phosphohydrolase enzymes was inversely correlated to dissolved inorganic phosphorus concentration. The particular characteristics of concentration kinetics obtained for PDE (saturation at 50 µM, high Km, high turnover times) are discussed with respect to possible inequal distribution of PDE and PME among organic material size continuum, and accessibility to phosphodiesters.

1 Introduction

Some species of phytoplankton and heterotrophic prokaryotes (Hprok) have the genetic ability to produce ectoenzymatic phosphatases that provide an important alternative source of P through extracellular hydrolysis of dissolved organic phosphorus (DOP). DOP is composed of various compounds having different degrees of bioavailability (Karl, 2014) including phosphate mono- and diesters (Kolowith et al., 2001; Yamaguchi et al., 2019). Determining ectoenzymatic activity using artificial fluorogenic substrates like methylumbelliferyl-phosphate is relatively simple and sensitive (Hoppe, 1983), and this method has been widely used in all oceanic regions to measure phosphomonoesterase (PME) activity (Su et al., 2023). Over large spatio-temporal scales, PME activity is usually regulated by dissolved inorganic phosphorus (DIP) with an increase of the activity when DIP concentration decreases. High rates of PME have been encountered in well-known P-limited environments like the Mediterranean Sea or the Sargasso Sea (Van Wambeke et al., 2002; Lomas et al., 2010, Pulido-Villena et al. 2021). Thus, PME activities have been extensively used as indicators of P deficiency (Sala et al., 2001; Van Wambeke et al., 2002, Labry et al., 2005; Lomas et al., 2010; Zaccone et al., 2012). However this inverse relationship between DIP concentration and PME activity is not systematic (Hoppe and Ulrich., 1999; Labry et al., 2016; Davis and Mahaffey, 2017; Duhamel et al., 2021; Lidbury et al., 2022), and questions raised about, for instance, the role played by the consortium of microorganisms present, the genetic nature of the phosphatase produced, its localization (i.e. periplasmic or truly dissolved), its dependence or not to metal ions and its promiscuity (Luo et al., 2009; Baltar et al., 2010; Mahaffey et al., 2014; Cerdan-Garcia et al., 2021; Srivastava et al., 2021; Lidbury et al., 2022). Kinetic parameters of PME have been also assayed using multiple concentrations of the substrate, providing additional information on maximum rates (Vm), half saturation constant (Km) and

turnover times (Km:Vm ratio) with respect to environmental conditions (Labry et al., 2005; Duhamel, et al., 2011; Suzumura et al., 2012; Pulido-Villena et al., 2021). The enzymatically hydrolysable fraction of DOP (here labile DOP, L_{DOP}) is defined as the DOP fraction hydrolyzed by a commercially available alkaline phosphatase, under optimal conditions of enzyme concentration, pH and temperature (Feuillade and Dorioz, 1992). The dynamics of both DIP and L_{DOP} have been investigated in the western North Pacific (Hashihama et al., 2013), or the central North Pacific (Yamaguchi et al., 2019), demonstrating the importance of L_{DOP} in supporting productivity in oligotrophic regions.

In addition to phosphomonoesters, phosphodiesters (P-diesters) constitute also an enzymatically hydrolysable pool in DOP. In aquatic environments, typical P-diesters identified are nucleotides, nucleic acids, and phospholipids coming from microorganism's intracellular material (Karl and Bjorkman, 2015), but the methodology used to estimate the P-diester pool (using also a commercially purified phosphodiesterase enzyme (Monbet et al., 2007; Yamaguchi et al., 2019) does not allow to determine the *in-situ* P-diesters chemical composition in detail. Phosphodiesterease (PDE) activity is also determined using artificial substrates like bis-4-methylumbelliferyl-phosphate, bis-paranitrophenyl phosphate or paranitrophenyl thymidine 5'monophosphate. PDE activity has been detected in cultures of marine heterotrophic bacteria (Dunlap and Callahan, 1993; Noskova et al., 2019), in a dinoflagellate culture causing harmful bloom (Huang et al., 2021) and in diatom culture (Yamaguchi et al., 2013). After enrichment of various chemical forms of organic phosphate added experimentally, the high changes in taxonomic diversity and activity of heterotrophic bacteria and phytoplankton (Muscarella et al., 2014; Sisma-Ventura and Rahav, 2019; Filella et al., 2022) as well as expression of different phosphatase genes (Zheng et al., 2019), suggest a strong role of the DOP availability in shaping microbial diversity in aquatic environments. Nevertheless, if PDE has been already measured in environmental conditions in eutrophic aquatic systems (Jorgensen et al., 2015) or coastal area (Huang et al., 2022), few studies describe PDE activity in oceanic waters, and only in the Pacific Ocean (Sato et al., 2013; Yamaguchi et al., 2019; Thomson et al., 2020; Srivastava et al., 2021).

The Eastern Mediterranean Sea is particularly impoverished in P relative to N, leading to high N:P molar ratios (Durrieu De Madron et al., 2011; Powley et al., 2017). The depth gap separating the two nutriclines increases eastward as the phosphacline deepens faster than the nitracline (Pujo-Pay et al.,

2011). Surface concentrations of DIP are typically under 50 nM (Djaoudi et al., 2018b), whereas nitrate is present at the surface after winter convection events which are strong enough to reach the nitracline (Ben Ezra et al., 2021; D'Ortenzio et al., 2021). Through enrichment experiments in situ, in minicosms or in bioassays, it has been shown that primary producers and heterotrophic prokaryotes within the surface layers of the eastern Mediterranean Sea are primarily limited by P, although this is sometimes accompanied by a colimitation with N for phytoplankton, and N or labile C for heterotrophic prokaryotes (Zohary and Robarts, 1998; Van Wambeke et al., 2002; Thingstad et al., 2005, Tanaka et al., 2011, Sisma-Ventura and Rahav, 2019). Consequently, P availability plays a major role in the microbial food web functioning in the eastern Mediterranean Sea.

We propose here an analysis of the concentration kinetic parameters, including the maximum rates, half saturation constant and turnover time, of the two types of phosphoesterases, PME and PDE, in the eastern Mediterranean around Crete during two distinct seasons: in autumn (October), chosen to represent typical warm and strong oligotrophic conditions, and at late winter (February-March), chosen to illustrate the productive conditions associated to episodic phytoplankton blooms. Our analysis aims to characterize the distribution of PME and PDE activities in link with the distribution of DOP, L_{DOP} and DIP in the epipelagic layers in this area, which is recognized as one of the most P-limited marine environment. A second paper in preparation (Van Wambeke et al., in prep) will be dedicated to PDE and PME distribution within the surface mixed layer in relation to mesoscale variability (cyclones vs anticyclones) and the progression of the phytoplankton bloom in winter.

2 Material and Methods

2.1 Sampling

Two cruises were conducted during the period 2018-2019: PERLE1 (11-20 October 2018) and PERLE2 (27 February-15 March 2019). These cruises were the basis for an extensive investigation of the western Levantine Sea carried out in the framework of the French program MISTRALS-Mermex and its component PERLE (Pelagic Ecosystem Response to dense water formation in the Levant Experiment, D'Ortenzio et al., 2021). During the autumn cruise PERLE1, the sampling plan focused on the warm

core of the anticyclone Ierapetra and its extensions in the Levantine Basin (Fig. 1). During the winter cruise PERLE2, the sampling plan extended over the whole area and a larger panel of dynamical features were encountered including the cold core of the Rhodes cyclonic Gyre located east of Crete (Fig. 2, more details in Taillandier et al., 2022).

For the purpose of this study, we sampled 11 stations during PERLE1 and 14 stations during PERLE2, corresponding to a large variety of hydrological situations (Table 1). For both cruises, full-depth oceanographic stations were carried out using a CTD-rosette equipped with a sampling system of 24 Niskin bottles and a Sea-Bird SBE9plus underwater unit equipped with pressure, temperature, conductivity, oxygen and chlorophyll fluorescence sensors.

Water sub-samples from the Niskin bottles were taken for nutrients (inorganic and organic, including nanomolar analyses of DIP and L_{DOP}), biological stocks (flow cytometry counts and chlorophyll a) as well as for phosphatase activities (PME and PDE).

At each station some selected layers were sampled: 10 layers for DIP with the sensitive technique and L_{DOP} (between 0 and 200 m during PERLE1 and 0 and 300 m during PERLE2, in link with nutrient and chlorophyll distributions in epipelagic water column), and among these, 6 layers for PME and PDE activities. Other nutrient analyses (nitrate, nitrite, DOP, DIP with the classical method) were sampled between surface and the bottom depth: 12 levels between surface and 300 m depth and 6 levels below 300m depth. However only the 0-300 m layer is described in this study.

2.2 Nutrients

Seawater samples for standard nutrient analysis were filtered online (0.45µm cellulose acetate filters) directly from the Niskin bottles in 20 ml acid-washed polyethylene vials and were stored frozen until analysis for PERLE1, and immediately analyzed on board for PERLE2. Micromolar nutrient concentrations of nitrate, nitrite and phosphate were determined by colorimetry (Aminot and Kérouel, 2007) using a segmented flow analyzer Seal-Bran-Luebbe (AAIII HR SealAnalytical©), with analytical precision of 0.02 µM, 0.01 µM and 0.01 µM, respectively.

Samples for the determination of nanomolar concentrations of DIP were collected in HDPE bottles previously cleaned with supra-pure HCl after filtration through 0.2 µm. During PERLE1, samples were stored frozen until analysis in the laboratory. During PERLE2, samples were analyzed on board immediately after sampling. Nanomolar DIP was analyzed using the LWCC method modified from Zhang and Chi (2002), with a detection limit of 1 nM.

Total dissolved phosphorus (TDP) was measured using the segmented flow analyzer technique after high-temperature (120 °C) persulfate wet oxidation mineralization (Pujo-Pay et al., 1997; Pujo-Pay and Raimbault, 1994). Dissolved organic phosphorus (DOP) was obtained as the difference between TDP and DIP.

The monoesterase hydrolysable fraction of DOP (L_{DOP}) was estimated after enzymatic hydrolysis of the < 0.2 µm filtrate in presence of a purified phosphatase alkaline (AP) enzyme from *Escherichia coli* (Sigma P4252) (Djaoudi et al., 2018a) in HDPE bottles. The AP was diluted with pure water to prepare a working solution of 0.2 U mL^{-1}. Equal volumes (0.6 mL) of AP working solution and Tris buffer (0.5 M, pH 8) were added to 30 mL of the < 0.2 µm filtered samples. Samples were then incubated during 3 h in the dark at 30°C. The duration of the incubation and the hydrolysis efficiency was checked with glucose 6-phosphate. After incubation, samples were stored frozen until analysis (PERLE1) or analyzed onboard (PERLE2). L_{DOP} was obtained as the difference in DIP concentration before and after incubation. A blank was run at each station consisting on 30 mL ultrapure water in which 0.6 mL of working AP solution and Tris buffer were introduced.

2.3 Biological stocks and fluxes

Flow cytometry was used for the enumeration of autotrophic prokaryotic and eukaryotic cells, heterotrophic prokaryotes (Hprok) and heterotrophic nanoflagellates (HNF). Water samples (4.5 mL and 2 mL) were fixed with glutaraldehyde grade I 25% (1% final concentration), flash frozen and stored at -80 °C until analysis. For Hprok, the 2 mL samples were defrosted at room temperature and subsequently analyzed using a FACSCanto flow cytometer (BD-Biosciences) of the BioPic platform (https://www.obs-banyuls.fr/fr/rechercher/plateformes/biopic.html) equipped with optics fiber emitted light (405, 488 and 633 nm). Fluorescent 1 µm beads for Hprok and 10 µm beads for HNF

(Polysciences Inc., Europe) were added to each sample as an internal standard to normalize cell properties and to compare cell populations. Accurate analyzed volumes and subsequent estimations of cell concentrations were calculated using Becton-Dickinson Trucount™ beads. Hprok and HNF cells, were discriminated and enumerated according to their right-angle light scattering properties (SSC, roughly related to cell internal complexity) and green (515-545 nm) fluorescence due to nucleic acid staining with SYBRGreen I (Molecular Probes) for 15 minutes at room temperature in the dark (Marie et al., 1997). Hprok were enumerated as the sum of 2 clusters (High Nucleic Acid content (HNA) and Low Nucleic Acid content (LNA) bacteria). Hprok biomass (Hprok-C) was calculated assuming 10 fgC per cell. Total HNF population was also discriminated following the same principle (Christaki et al., 2011).

Phytoplankton Samples were analysed according to Marie et al. (2000) protocols using the FACSCalibur (BD Biosciences ®) of the PRECYM flow cytometry platform (https://precym.mio.osupytheas.fr/), equipped with a blue (488 nm) laser and a red (634 nm) laser. Just before phytoplankton analyses, 2 µm beads were added as an internal standard and to discriminate picoplankton (< 2-3 µm) and nanoplankton (> 2-3 µm) populations (Fluoresbrite YG, Polyscience). A Trucount beads (BD Biosciences ®) solution was also added to the samples to determine the volume analysed. The same sample was acquired twice using two different settings: the first one to assess picophytoeukaryotes (Picoeuk), nanophytoeukaryotes (Nanoeuk) and cryptophyte-like cells (Crypto) and the second one, using a higher amplification of the photodetector of the red fluorescence signal (induced by chlorophyll), was set to focus on the small size and/or cells with low chlorophyll *a* fluorescence, such as *Prochlorococcus* (Pro) and *Synechococcus* (Syn). The cell concentration was determined from both Trucount beads and flow rate measurements. Total chlorophyll a (Tchla) is the sum of chlorophyll a and divinyl chlorophyll a. It was calculated by HPLC analysis after extraction of pigments from GF/F filters (Ras et al, 2008). The fluorescence sensor was calibrated with Tchla. The total phytoplankton biomass (phyto-C) was calculated assuming an overall C:Tchla ratio of 50.

Ectoenzymatic activities were measured fluorometrically with fluorogenic model substrates (Hoppe, 1983), using 4-methylumbelliferyl-phosphate (MUF-P, Sigma) and bis(4-methylumbelliferyl)

phosphate (bisMUF-P, Chem. Pex) to assess phosphomonoesterase (PME) and phosphodiesterase (PDE) activities, respectively. The release of MUF from fluorogenic substrates was monitored by measuring the increase of fluorescence in the dark (excitation/emission 365/450 nm, wavelength bandwidth 5 nm) periodically (at least 5 times) during up to 12 h using a VARIOSKAN LUX microplate reader. The 24-well microplates were incubated in a thermostatic incubator at *in situ* temperature, in the dark. Aliquots (2 ml) of sample were incubated with final concentrations of fluorogenic substrates varying from 0.025 to 1 µM for MUF-P, and from 0.025 to 50 µM for bis-MUF-P. These ranges were chosen after preliminary tests using 0.025 to 50 µM concentrations for both activities. The parameters Vm (maximum hydrolysis velocity) and Km (Michaelis-Menten constant that reflects enzyme affinity for the substrate) as well as their corresponding errors were estimated by non-linear regression (software PRISM, https://www.graphpad.com/features) using the Michaelis-Menten equation:

$$V = \frac{Vm\ x\ S}{Km+S} \quad (1)$$

where V is the hydrolysis rate and S the fluorogenic substrate concentration added. Turnover times (TT) were calculated as Km/Vm ratio.

2.4 Data processing and diagnostics

Measurements by CTD sensors were processed into 1-m resolution vertical profiles for in-situ temperature, salinity, potential density anomaly referenced to surface (shortened to density hereinafter), and calibrated chlorophyll fluorescence. The mixed layer depth (MLD) was determined as in Taillandier et al. (2022). The depth of the nutriclines were calculated from DIP and NOx vertical profiles. The nitracline depth (Ncline) was estimated by the intercept of the regression line reported in a NOx versus depth diagram, and the phosphacline (Pcline) by the intercept of the regression line reported in a DIP versus depth diagram, in which we used the DIP concentrations determined with the LWCC technique for depleted layers and classical DIP measurements for richer layers (> 0.08 µM). The least square regressions were made on the linear parts of the plots of NOx and DIP versus depth.

3 Results

3.1 Distribution of physical properties

During wintertime situation (PERLE2 cruise), sea surface temperature ranged from 15.5 to 17.4 °C (Table 1). The vertical gradient of temperature between the surface and 300 m depth was weak (maximum difference of temperature 2.4°C). Density profiles (Fig. S1) showed i) very well mixed surface layers at stations 1, 13, 15 - sampled at the beginning of the cruise in the Cretan Sea including the Kythira strait - and station 50, located south of Crete in the center of an anticyclonic gyre (Fig. S1b); ii) slightly mixed conditions: st104-108 located in the Kassos and Karpathos straits along the anticyclonic side of the geostrophic jets entering in the Cretan Sea, and iii) the other stations of PERLE2 cruise showed variable degrees of stratification during the progression of the cruise toward the east and the Rhode Gyre (Fig. S1c).

The MLD varied over a large range, between 14 m and 269 m (mean ± sd: 83 ± 69 m, Table 1). The highest MLD were encountered in the Cretan Sea (st 1, 13, 15) and in the center of an anticyclone south of Crete (st 50, Fig. 2, Fig. S1b). In contrast, some stations sampled along the easternmost transect (e.g. st 80 and 94) were located in extensions of the Rhodes Cyclonic Gyre and presented lower MLD (Fig. 2, Fig. S1c, Table 1).

In the autumn situation (PERLE 1 cruise), density profiles were more similar among stations because the stations were sampled in a more restricted area within the anticyclone Ierapetra (Fig. 1). Sea surface temperatures ranged from 26.5 to 27.8 °C (Table 1), with an important thermal and density stratification (Fig. S1a). The mean MLD (35 ± 19 m, Table 1) was significantly lower than in the winter situation (Mann Whitney test, $p = 0.012$).

3.2 Nutrients

In winter, the depth of the Pcline was on average 124 ± 76 m, showing a great variability among stations (Fig 3b, c). In autumn, vertical distributions of DIP showed depleted values in the mixed layer and a rapid increase with depth, with Pcline depths being more homogeneous than in winter, and reaching on average 154 ± 43 m (Table 1, Fig. 3a), although the difference between both cruises was not statistically different ($p = 0.10$). The same trend was observed for vertical profiles of NOx (the sum

of nitrate+nitrite): greater variability in winter, homogeneous profiles of concentrations in autumn (Fig. 3 d, e, f), with however significant deepening in autumn ($p = 0.044$), with Ncline depth being reached at 124 ± 30 m in autumn versus 80 ± 75 m in winter. In winter, the deepest Ncline and Pcline (Table 1) were observed in the stations situated within anticyclonic areas (st 50, 108) followed by the well mixed conditions at the beginning of the cruise (st 1, 13, 15). The shallowest Pcline and Ncline were reached at st 80 and 94. In all cases (except one), Pcline was deeper than the Ncline with an average difference of 44 ± 26 m in winter and 29 ± 21 m in autumn (statistically not different; Mann Whitney test, $p > 0.05$). During the winter cruise, DIP in the ML was higher in the Cretan Sea (average concentration 20-24 nM at st 1, 13 and15, Table 2). DIP in the ML was on the same order of magnitude in the rest of the stations of the the winter cruise (8-12 nM) and at all the stations during the autumn cruise (8-13 nM). Consequently, DIP concentrations were not particularly lower within the ML in the autumn oligotrophic situation (Fig. 3a) and DIP concentrations between PERLE1 and PERLE2 were not statistically different ($p = 0.6$). This was not the case for NOx which clearly showed N-depleted conditions within the ML in autumn (with means significantly lower than in winter, $p < 0.001$), with frequent subsurface data below the threshold of detection of 0.01 µM (mean concentrations in the ML ranged 0.01-0.03 µM, Table 2, Fig. 3d). In winter, NOx varied on a large range, means of concentrations per station inside ML being higher in the Cretan Sea (st 1, 13, 15: 0.99-1.13 µM) and anticyclonic areas (st 111, 116: 0.79-0.61 µM). At the opposite NOx showed lower values in the ML at some other stations mostly situated on the easternmost transect (st 35 ,75, 90, 94: 0.22-0.32 µM), (Table 2, Fig. 3f). The ratio of NOx to DIP within the ML was significantly ($p < 0.001$) higher in the winter situation (55 ± 19 vs 1.8 ± 0.7, Fig. S2).

For the whole data set, the ranges of DOP and L_{DOP} were 8-92 nM and 1-17 nM, respectively, during autumn and 10-120 nM and 2-64 nM, respectively, during winter (Fig. 4 a,b,c). The higher values of L_{DOP} (> 25 nM) were encountered on few cases during winter in the Cretan Sea and at st 75, for the remaining data set, values were all below 25 nM (Fig. S3). For the whole data set, DIP and DOP explained no or low variability of L_{DOP} (Fig. S3, $r^2 < 0.06$ for all tests on log-transformed data). For the whole data set, the fraction of L_{DOP} in DOP (%L_{DOP}) varied on a large range, from 1.3% to 97%, with a mean of 28% ± 18%.

Within the ML, means of DOP and L_{DOP} per station were significantly lower during the autumn cruise: DOP means being 25 ± 10 nM vs 50 ± 16 nM ($p < 0.001$); and L_{DOP} means being 6 ± 2 vs 16 ± 9 nM ($p < 0.001$).

3.3 Chlorophyll stocks and phytoplankton populations

In autumn, vertical distribution of chlorophyll stocks were homogeneous, showing low values in surface (0.02 - 0.07 µg Tchla l^{-1}) and deep chlorophyll maximum (DCM) visible around 84-125 m depth which peaked up to 0.2 µg Tchla l^{-1} (Fig. S1d). In autumn, integrated chlorophyll stocks were low (16 ± 4 mg Tchla m^{-2}). In winter, at stations under deep ML conditions, Tchla stayed homogeneous down to 300 m (st 1, 13 15 and 50) and showed a small decrease with depth at st 104 and 108 (Fig. S1e). In other stations of the winter cruise, diverse shapes of Tchla vertical distribution were seen, with surface or subsurface peaks varying from 0.25 (st 21) up to 0.95 (st 80) µg Tchla l^{-1}. Integrated stocks were on average significantly higher during the winter cruise (50 ±14 mg Tchla m^{-2}, $p < 0.001$) showing a greater variability than in the autumn cruise, with maximum values (> 60 mg Tchla m^{-2}) reached at st 15 and 50 (mixed stations) and at some other stations sampled at the end of the cruise and/or under Rhode gyre or anticyclonic influence (st 58, 80, 108, 111, Fig. S1f, Table 1).

In autumn, all picophytoplankton groups were more abundant than in winter. *Prochlorococcus* abundances peaked within the DCM depth with maxima varying according stations between 23 and 47 x 10^3 cells ml^{-1} (Fig. S4a) whereas pico- eukaryotes where rather peaking within the surface (0.13 - 0.68 x 10^3 cells ml^{-1}, Fig S5a) and *Synechococcus*-like abundances within the subsurface layers (7.9 - 19 x 10^3 cells ml^{-1}, Fig. S4d). Heterotrophic prokaryotes also peaked within the DCM depth with abundances at the peak ranging 3.6– 5.4 x 10^5 cells ml^{-1} (Fig. S6d). In winter, following mixing/stratification conditions, all phytoplankton groups (Syn, Proc Picoeuk, Nanoeuk, crypto) as well as Hprok were low and relatively homogeneous along the vertical profile at st 1, 13, 15, 50, 104 and 108 (Figs. S4 b, e; S5 b, e; S6 b, e). Proc showed variable profiles for the other stations of PERLE2 cruise, with surface or subsurface peaks (st 68, 90, 111, Fig. S4c). Syn followed Proc vertical trends, and peaked also within the surface of subsurface (Fig. S4f). Vertical distribution of Picoeuk abundances also

varied along the different profiles, peaking between surface and 100 m (Fig. S5c). Nanoeuk followed same vertical trends than Picoeuk, with maximum abundances up to 140 cells ml^{-1} reached during PERLE1 cruise, Fig. S5f). Cryptophyte-like cells were scarce, but notably showed small surface abundance peaks during the winter cruise at some specific stations (st 80, 90, Fig. S6c). Finally, vertical profiles of Hprok (Fig. S6d, e, f) varied also in shape and order of magnitude of abundances reached, with Hprok abundances at the peak ranging 3.2 - 7.3 x 10^5 cells ml^{-1}.

3.3 Phosphomonoesterase and diesterase activities

For PME, 20 kinetics and for PDE, 41 kinetics over 174 were not available due to the low increase in fluorescence with time after addition of low concentrations of MUF-P or bis-MUF-P. These were generally situated within the deepest layers sampled. After testing a large set of substrate concentration between 25 nM and 50 µM on some samples, the saturation state was reached at different concentrations for PME and PDE (Fig. 5). PME reached their maximum activities (Vm) after 1 µM MUF-P addition whereas it was necessary to add up to 50 µM bis-MUF-P to reach saturation state with PDE. Consequently, the affinity constants (Km) were higher for PDE (Fig. 6a). On average for the whole data set, the Km PDE was 33-fold higher than that of the PME (mean ± sd : 33 ± 25), however Km PME and Km PDE were not correlated. Km PDE decreased with depth during both cruises (Fig. 6 d, f), except at the well mixed stations 1, 13, 15 in February-March (Fig. 6 e) At the opposite, Km PME either increased with depth (autumn cruise, Fig 6 a) or did not vary with depth (winter cruise, Fig 6 b, c). Neither Km PME, nor Km PDE, correlated with DOP or L_{DOP}, whatever the cruise (log-log relationships tested, $p > 0.05$). On the other hand, Km showed variable correlations with DIP depending on the cruise or the enzyme: Km PDE decreased when DIP increased during both cruises, and Km PME increased when DIP increased in October whereas this relation was insignificant in February-March (Fig. 7a).

Within the ML, Km mean per station ranged from 1.10 to 7.58 µM for PDE and from 0.054 to 0.288 µM for PME (Table 3). Km PME within the ML were significantly different between PERLE1 and PERLE2 cruises (0.066 ± 0.008 µM and 0.169 ± 0.060 nM; Mann Whitey test, $p < 0.001$). This difference was insignificant ($p = 0.06$) for Km PDE (3.45 ± 1.85 µM and 4.56 ± 2.25 µM). Within the

ML, PDE Km were the lowest in winter for the well mixed stations (st 1, 13, 15) but reached their maxima at stations toward the Rhode gyre (st 80, 90, 94, 111, 113) and the eastern Straits (st 104-108, Table 3).

For the whole data set, PME and PDE potential rates (Vm) ranged 0.04-18.9 nmol l^{-1} h^{-1} and 0.017-23.4 nmol l^{-1} h^{-1} respectively, in winter; and on a much lower range in autumn (0.014-2.7 nmol l^{-1} h^{-1} for PME Vm and 0.011-5.7 nmol l^{-1} h^{-1} for PDE Vm). Vm of both types of phosphatases decreased with depth rapidly below the ML (Fig. 4 d, e, f). Contrarily to the Km values, Vm PDE and Vm PME were on the same order of magnitude (ratio Vm PME:Vm PDE, mean ± sd 1.1 ± 0.9, range 0.26-6.29, Fig. S2). Both rates were linearly positively correlated particularly in winter, when the data range was larger (Vm PDE = 1.38 x Vm PME + 0.54, $r^2 = 0.93$, $p < 0.0001$ in winter; Vm PDE = 1.32 x Vm PME - 0.29, $r^2 = 0.56$, $p < 0.0001$ in autumn; plots not shown). DOP and L_{DOP} explained mostly no variability of Vm PME, or Vm PDE, whatever the cruise (log-log relationships tested). At the opposite, Vm decreased as DIP concentration increased in all cases, the relations being highly significant for both cruises and phosphatase types (Fig. 7b) but with lower determination coefficients in autumn (Table S1). The slopes were significantly different between the 2 cruises (Feb-March vs October) only for Vm PME (*F*-test, $p < 0.05$) but not for Vm PDE. The slope of the Vm PME-DIP relationship was significantly lower than that of the Vm PDE-DIP relationship only for the Feb-March cruise (*F*-test, $p < 0.05$). Note that the log Vm = f(log NOx) relationships were also highly significant during both cruises and for both types of phosphatase (for the 4 regressions, $p < 0.001$, plots not shown). In autumn, the NOx:DIP ratio was positively correlated to the ratio Vm PME:Vm PDE (log-log regression, $r^2 = 0.40$, $p < 0.001$). On the other hand in winter, when NOx was more available within the ML, it did not explain any variability of the Vm PDE:Vm PME ratio ($r^2 = 0.04$, $p > 0.05$). The turnover times (ratio Km:Vm) of PME and PDE ranged 0.6-257 days and 11-1593 days (mean ± se 25 ± 45 and 174 ± 317 days), respectively.

Within the ML, means of both Vm PME and Vm PDE per station were the lowest at st 1, 13, 15 in the Cretan Sea in winter and peaked at stations 80, 90 and 94 on the easternmost transect. (Table 3), revealing a great variability during the winter cruise. Within the ML, Vm were not particularly higher during the autumn cruise despite the high *in situ* temperature difference, and means per cruise were not

statistically different: for Vm PME (2.2 ± 0.4 nmol l^{-1} h^{-1} in autumn, 5.0 ± 5.1 nmol l^{-1} h^{-1} in winter, p = 0.13), and for Vm PDE 2.9 ± 1.3 nmol l^{-1} h^{-1} in autumn, 7.6 ± 6.8 nmol l^{-1} h^{-1} in winter, p = 0.06).

We calculated specific PME and PDE activities by normalizing over abundances of Hprok, Tchla as well as a proxy of total living carbon biomass determined as the sum of hprokC + phytoC (see methods). As for Vm, all kinds of specific Vm decreased with increasing DIP concentrations, and all the relations were significant for both cruises and phosphatase types (Table S1).

Mostly, log - log regressions between Vm rates of both types of phosphatases and cell abundances of each identified phytoplankton cytometric group were significant when each population was considered individually (Tables S2, S3). Conversely, relations were insignificant, or presented a low r^2 (< 0.27) for heterotrophs (HNA, LNA total Hprok or HNF). To avoid autocorrelations between variables (Vm rates and abundances of all cytometric groups tended to decrease with depth) we also examined partial correlations coefficients using multiple log-log regressions, using all cytometric groups as independent variables. Cryptophyte-like cells and *Synechococcus* were the two populations explaining variability of Vm PME during PERLE2 cruise, whereas it was picophytoeukaryotes and *Synechococcus* during PERLE1 cruise (Table S2). For Vm PDE, it was the same 2 populations for PERLE2 cruise as for Vm PME, expect that it was only *Synechococcus* for PERLE1 cruise (Table S3). Abundances of LNA cells, HNA cells and HNF cells never significantly explained any variability of Vm rates in the multiple regressions.

4 Discussion

4.1 Phosphate pools and P stress

During both cruises, DIP showed classical nutrient profiles with depleted DIP within the surface layers and increasing values at depth. DIP stocks showed low values within the upper layers: means in the mixed layer varying from 5 to 24 nM according stations. Over a larger spatial scale in the Mediterranean Sea, Pulido-Villena et al. (2021) obtained 6-15 nM in spring in the phosphate-depleted layer across the Ionian and Western Basins and over a large time scale, values were reported ~ 6 nM throughout the entire year in the Levantine Sea (Ben Ezra et al., 2021).

L_{DOP}, the pool of DOP hydrolysable by a phosphomonoesterase purified from *E Coli*, was lower than 25 nM, except for a few samples, and were in the same range than in above-nutricline waters of the Central North Pacific (from DL to 40 nM, Yamaguchi et al, 2019). The L_{DOP} depth profile pattern did not matched that of DIP: L_{DOP} displayed constant values with depth with no particular peak within the DCM. A shift towards a nutrient like distribution has been reported only in some of the coastal stations examined by Hashihama et al. (2013) who suggested these were under severe P stress. At the opposite, Yamaguchi et al. (2019) showed constant profiles or occasionally higher L_{DOP} peaks within the 0-100 m layer within the low to middle latitudinal central North Pacific, along a transect including stations under moderate P stress. L_{DOP} concentrations were shown to be lower at the basin scale under low (< 100 nM) DIP conditions when compared to > 100 nM conditions in the moderate P stressed area explored by Yamaguchi et al. (2019) in the Pacific. Conversely, in our study, there was no significant linear correlation between L_{DOP} and DIP (Fig. S3), but our DIP concentrations varied on a lower range (mean ± sd 36 ±48 nM) , and all the data in the ML were below 26 nM.

The fraction of L_{DOP} in DOP (%L_{DOP}) varied on a large range, from 1.5% to 97%, with a mean of 28% ± 18%. This mean is in the same range as in Djaoudi et al. (2018a) (27 ± 19 %) in a year survey of epipelagic layers in the western Mediterranean Sea (ANTARES offshore station). It was on average lower (7 ± 5%) in a moderate P stress oceanic area (Pacific, Yamaguchi et al 2019), but as variable as along a salinity gradient in the DIP rich (0.3-1.9 µM DIP) Tamar estuary (Monbet et al., 2009: 0.7 to 79%, mean 35% ± 21%).

L_{DOP} accounted for a large and variable percentage of the DOP pool, suggesting that other components of the DOP might play a role in P cycling. The variability of the PDE Vm and Km estimated in our study suggests that P-diesters could be an important P source for marine microorganisms. Marine P-diesters, like P-monoesters, have been quantified based on hydrolysis of DOP by purified enzymes (Suzumura et al., 1998, Monbet et al., 2009; Yamaguchi et al., 2019). Although no data has been quantified to date in the Mediterranean Sea, other measurements suggest that P-diesters could represent as much as P-monoesters. In a nutrient rich estuary (DIP ranged from 0.28 to 1.2 µM) under strong salinity gradients and interaction with sediment porewaters, P-diesters contributed on average 29% of the DOP compared to 35 % for P-monoesters (Monbet et al., 2009). Along 170° North in the Pacific

Ocean, marine P-diesters in epipelagic layers (on average 5 ± 6 nM) are lower than P-monoesters (on average 12 ± 5 nM) (Yamaguchi et al., 2019). P-diesters include a large panel of molecules as nucleic acids, nucleotides, or phospholipids. Among these forms, phospholipids P concentration ranged 0.6-25 nM in coastal areas (Suzumura and Ingall., 2001). From Goutx et al. (2009), dissolved phospholipids in Mediterranean Sea amounted on average around 1 µg C l^{-1} and up to 3.7 µg C l^{-1}. Based on an average C16 for the fatty acid chain length, P would represent around 6.8 % of the phospholipid carbon mass, i.e dissolved phospholipids would be around 2.2 nM P, up to 8 nM, which could be considered as minimal ranges of P-diesters concentrations, as they include also other P-diesters types. Thus, both P-monoesters and P-diesters should be considered in the P cycle in the Mediterranean Sea.

4.2 Phosphatase kinetics

Our study is the first one describing simultaneously PME and PDE activities in the Mediterranean Sea. Furthermore, to our knowledge, this is the first study describing systematically Michaelis-Menten equations for PDE until saturation state. Indeed, both types of phosphatases displayed typical Michaelis-Menten kinetics, but PME saturated after addition of 1 µM MUF-P and PDE saturated only after 50 µM addition of bis-MUF-P. Kinetic parameters Vm and Km are thus difficult to compare with previous literature, as Km and Vm depend on the range of concentration of fluorogenic substrates added, with recommendations to add up to 10 times the Km value to calculate Vm appropriately (Urvoy et al., 2020). In most cases only one single substrate concentration is used: for instance, Sato et al. (2013) compared PME and PDE rates using 1 µM substrate concentration, Thomson et al. (2020) used 100 µM concentrations and Huang et al. (2022) 1 mM. In addition, while some authors used MUF-derivatives (Sato et al., 2013; Thomson et al., 2020), others used paranitrophenyl-derivatives (Huang et al., 2022), corresponding probably to different enzyme affinity. In addition, conditions of incubation may also differ, some authors using *in situ* or close-to *in situ* temperature (Sato et al., 2013; Suzumura et al., 2012; Yamaguchi et al., 2019; Thomson et al., 2020) and others optimal temperatures (Huang et al., 2022).

Sato et al. (2013) and Suzumura et al. (2012) explored PME activities at 10 m and at the DCM depth in the North and south Pacific Ocean, where DIP concentrations varied from 3 nM to hundreds of nM.

They did some kinetics with PME up to 1 µM MUF-P concentrations, and thus their results are comparable to ours for this enzyme: they found maximum PME hydrolysis rates (Vm) reaching at best 3.7 nmol l^{-1} h^{-1} .In our study we obtained values up to 18 nmol l^{-1} h^{-1}, confirming the other high values already obtained in western and central Mediterranean Sea in spring or in winter in the open sea (up to 13 nmol l^{-1} h^{-1}, Van Wambeke et al., 2002; 2021). PDE Vm seems to range also in the same order of magnitude than PME Vm. Thomson et al. (2020) measured PDE and PME potential rates at 100 µM concentrations, at a station in the South Pacific located 65 km off the Otago coast, in subantarctic waters. In the surface (2 m), 500 m and 1000 m depths explored in their study, DIP was always detectable (0.5-1 µM). The 2 m depth layer presented seasonal variations, with PME rates varying 2.7-12 nmol l^{-1} h^{-1} and PDE rates 1.4-20 nmol l^{-1} h^{-1}. The comparison of this study with others previously assessing PME and PDE activity rates (Sato et al. 2013, Thomson et al. 2020) reveals similar patterns. Indeed, in all cases, Vm was on the same order of magnitude for both phosphatase enzymes and their variability was better explained by DIP than by DOP or LDOP. This similarity of patterns among oceanic regions occurs despite contrasting environmental conditions. The Subantarctic waters sampled by Thomson et al. (2020) are located in a HLNC region rich in macronutrients (DIP ranged 0.5-18 µM) and poor in trace metals. At the opposite, part of the region covered by Sato et al. (2013) (the North West Pacific) is not iron-limited but P-limited (Liang et al., 2022), similarly to the Eastern Mediterranean Sea (Statham and Hart, 2005; Thingstad et al. 2005), although phytoplankton in the eastern MS can be N+P co-limited and heterotrophic prokaryotes labile C+P co-limited (Van Wambeke et al., 2002; Thingstad et al., 2005; Tanaka et al., 2011). In the North Pacific, nitrogen fixation occurs and is mainly expressed by cyanobacterial diazotrophs like *Trichodesmium* and *Crocospharea* (Horii et al., 2023). In the eastern MS, dinitrogen fixation represents a small contribution to primary production (Rahav et al., 2013) and is expressed essentially by heterotrophic prokaryotes. Further, these heterotrophs are rather controlled by organic C availability than by iron (Sisma-Ventura et al., 2019). Finally, it is in the eastern MS that the lowest DIP turnovertimes have been measured (< 10 h, Talarmin et al., 2015) compared to the South West Pacific (10-100 h, Van Wambeke et al., 2018) or the North Pacific (48-939 h, Sohm and Capone, 2010 and references therein.

In Thomson et al. (2020) study, the ratio of rates PME:PDE in surface was lower or higher than 1 (range 0.5 to 5.3) and varied seasonally. Their surface values were linearly correlated negatively with DIP and positively with the NOx:DIP ratio. In our study, the NOx:DIP ratio in the ML was on average much lower in autumn than in winter (1.8 ± 0.7 compared to 55 ± 19), traducing possibly different degree of limitation (N+P co-limitation in autumn, P limitation in winter). Over our whole data set, the ratio Vm PME:Vm PDE was not related to DIP or to the ratio NOx:DIP. Only under autumn conditions a positive correlation was observed between the ratio Vm PME:Vm PDE and the ratio NOx:DIP , similarly to what was observed by Thomson et al. (2020). Intuitively, it is expected that heterotrophic bacterial communities and/or some phytoplankton groups would develop more nucleotidases, DNase, or RNases relative to monoesterases when NOx becomes also limiting in regard to DIP, as such types of PDEs allow access simultaneously to both organic P and N sources. As in our study the correlation between Vm PME:Vm PDE and NOx:DIP ratio in autumn was estimated including all data, this relationship must consider also NOx:DIP changes along the vertical column. Indeed, NOx:DIP ratio increased within the DCM layer, associated to higher Vm PME:Vm PDE ratios. Within the DCM, besides lower light, the N source is more energetically available (i.e. reduced) due to nitrification process, and nitrate is more available as Ncline is shallower than the Pcline. Moreover, Thomson et al. (2020) suggested also that the variability of Vm PME:Vm PDE could traduce shifts in communities expressing different genes or in the availability of different P esters. As a consequence of being recognized a different biogeochemical niche, the DCM layer present also different communities of phytoplankton and heterotrophic bacteria than in the ML layers (Scharek and Latasa, 2007; Dupont et al. 2015; Estrada et al. 2016, Crombet et al., 2011), i.e. different populations possibly having different types of genes expressing phosphatase activities. During the winter cruise, multiple regression revealed that *Synechococcus* and Cryptophyte-like cells were mostly explaining the variability of Vm PME and Vm PDE. Further, we probably could not determine accurately the abundances of *Prochlorococcus* cells by flow cytometry despite the special setting of the machine used to specifically enhance the detection of this population having very dim fluorescence in surface, particularly in autumn, when dv-chla was above the limits of detection in the mixed layer. This is a very common feature already described in the

literature (Mella-Flores et al., 2011; Reich et al., 2022). Based only on multiple regression analysis, it is difficult to establish a causal link between phytoplankton groups and phosphatase activities.

Sato et al. (2013) and Suzumura et al. (2012) found Km PME ranging from 0.08 to 1.3 µM in the Pacific Ocean. Yamaguchi et al. (2019) in the North Pacific used more systematically MUF-P concentration kinetics up to 2 µM along vertical profiles, and obtained Km ranging from 0.095 to 1.9 µM. Data in our study were in the lower range of the above cited publications. It is however possible that we achieved higher sensibility for Km determination as we performed concentration kinetics with 6 concentrations starting at 0.025 µM MUF-P. Sato et al (2013) from their small data set (10 kinetics), observed a positive relationship between PME Km and DIP, which was considered as an environmental adaptation through production of ectoenzymes with higher affinity for the substrate (i.e. low Km) when the degree of P deficiency increases (i.e. low DIP). In this study, the strong stratified conditions in the post bloom situation within the Ierapetra gyre led effectively to a lowering of Km PME and of L_{DOP} inside the ML compared to the winter cruise (Tables 2 and 3), and thus a better affinity for substrate for PME in autumn when L_{DOP} is low. Going further with the data set per cruise over the water column, we found either none (Feb-March cruise), or a positive relationship (October cruise, Fig. 7a) between Km PME and DIP concentrations, showing that Km does not always follow the Sato et al. (2013) concept. Furthermore, a consistent fact in comparison with the few authors that used MUF-P concentration kinetics simultaneously with measurements of the different DOP pools is that Km PME was neither related to DOP nor to L_{DOP} concentrations, i.e. confirming that the DIP is the driving force for PME activity, not the enzyme substrate source. As previously discussed, it is possible that L_{DOP} does not reflect the real conditions of accessibility to the substrate pool (Duhamel et al., 2011; Suzumura et al., 2012). Indeed, why microorganisms would express enzymes having kinetic properties with PME Km being about 13-fold higher than L_{DOP} stocks? Possibly intermittent sources and patchiness of L_{DOP} composition and concentration could explain high Km relative to L_{DOP} so that microorganisms maximize their PME activities at high L_{DOP} concentrations. Patchiness is the consequence of the organic matter continuum of size with different molecular composition from low molecular weight to high molecular weight (Young and Ingall, 2010). Patchiness is provoked for instance, during the passage of sedimenting particles with their associated plumes (Kiørbe et al., 2001, phases of intense lysis of cells,

egestion of food vacuoles by grazers (Nagata and Kirchman, 1992), or hydrolysis of particulate detritus. In addition, since most PME comes from intracellular or periplasm of cells (Luo et al., 2009), they are probably adapted to higher concentrations of DOP than that estimated by the bulk DOP measurement. Other caveats could be linked to the representativity of an artificial fluorogenic substrate, or the difficulty to assess PME activity under few nM concentrations of MUF-P (Pulido-Villena et al., 2021). For Km PDE, Sato et al. (2013) found no correlation with DIP whereas we found a negative one, observed in winter as well as in autumn (Fig. 6a), i.e. the affinity for PDE substrate increases when DIP increases, which is counterintuitive as long as we consider DIP as a proxy for P limitation, and as long as we consider that PDE is induced under P stress. Such negative correlations could be related to the depth effect: indeed, Km PDE tended to decrease with depth and it was not the case for the Km PME. Thus, the variability of Km PDE with depth could be linked to probable changes over the epipelagic layers in nutrient stress (P vs N+P), in the composition of natural PDE substrates and/or in the presence of different types of PDE according the consortium of microorganisms present, as discussed above for Vm PME:Vm PDE ratio.

4.3 Bioavailability of organic P

As a consequence of the great difference in Km, the turnover time (TT) of the P-diester pool was ~ 7 times higher than for P-monoesters (TT means 26 days for PME, 175 days for PDE). PDE and PME turnover times are difficult to compare considering the different range of concentrations used in the other field studies, but most authors agree for a higher TT for PDE. In Sato et al. (2013) TT PME ranged 5-112 days, i.e. about one order of magnitude lower than for PDE (128-535 days), with concentration kinetics up to 1 µM fluorogenic substrate. In Yamaguchi et al (2019), expanding their data in the Pacific down to the equator, mean TT were 99 ± 75 days for PME and 2944 ± 1224 days for PDE, with concentration kinetics using up to 2 µM fluorogenic substrate. A higher PDE turnover time suggests that P-diesters are a slowly degradable fraction of the DOP. However, P-diesters include a large panel of molecules which might have different turnover times based on their chemical nature and solubility. A methodological bias explaining a high PDE TT is that the substrate used, bis-MUF-P seems not to be efficiently hydrolyzed using a purified PDE type I from venom whereas other artificial

P-diester substrate as p-nitrophenyl thymidine 5'monophosphate (pNP-TMP) are hydrolyzed under the same conditions (Yamaguchi et al., 2019). The inconvenient is that the hydrolysis of pNP-TMP is followed by colorimetry, resulting in a much less sensitivity than with bis-MUF-P which hydrolysis is followed by fluorimetry, and then does not allow to run concentration kinetics with very low concentration of substrates. The bias seems also to be present using another artificial substrate, as bis(paranitrophenyl) phosphate was only partly hydrolyzed in conditions where DNA was almost fully hydrolyzed (Monbet et al 2007, Turner et al., 2002).

The high molecular weight (HMW) fraction of the DOP was submitted to enzyme digestion by purified PME and PDE in coastal seawater off the Tokyo Bay (Suzumura et al., 1998). In this study, HMW fraction contained one third of the total DOP pool and 5 times more P-diesters than P-monoesters (7% P-monoesters, 48% P-diesters and 44% non-reactive DOP), which confirmed an inequal distribution of P-diesters compared to P-monoesters. Accessibility to the P-diesters for the enzymes plays also a role on its degradability as P-diesters might be embedded in HMW fractions such as colloids, virus-like particles, vesicles or sub-micron particles (Biller et al., 2022), so that P-diesters could be not accessible to the purified enzyme during the assay, as discussed in Suzumura et al. (1998) and Monbet et al. (2007). Possibly, the localization of natural enzymes also differs along the organic matter size continuum as it has been shown for bacterial phosphatases (Luo et al., 2009), although to date PME and PDE activities were equally distributed based on studies using size fractionation: Thomson et al. (2020) found mostly and equal (87-88%), cell-free (< 0.2 µm) proportions of PME and PDE activities in cold, subantarctic waters (87-88%), and Huang et al. (2022) in a temperate, rich coastal area under bloom conditions found mostly high proportions in the nano-micro (> 2 µm) size fraction for both enzymes (> 74%). The long turnovertimes of PDE obtained in our study whatever the season, stratification conditions, N or N+P degree of limitation, suggest that P-diesters are more stable than P-monoesters, although care should be taken to determine in future studies the accessibility to the substrate by the enzyme and the representativity of analog substrates.

5 Conclusion

This is the first study showing the distribution of both phosphomonoesterase and phosphodiesterase in the Mediterranean Sea, via systematic use of concentration kinetics. This approach avoids biases linked to the use of single concentration or range of concentration not adapted to Vm PDE estimates. This study confirmed the general trend obtained in other studies, i.e. that Vm PDE and PME rates seem to be more controlled by DIP availability rather than by the substrate availability. Although DIP concentration remained more or less constant within the surface mixed and DIP-depleted layer, the large changes of Vm rates and percentages of L_{DOP} obtained according stations and seasons, suggests strong adaptations of microbial populations and large degrees of P limitation. The much higher Km and turnover-times obtained for PDE compared to PME suggests different accessibility to the substrate P-monoesters and P-diesters along the organic matter size continuum. Opposite changes of the kinetic parameters of PDE and PME (Km values, Vm PME: Vm PDE ratio) with depth, suggests adaptations of the microorganisms producing them along the epipelagic layer as they are submitted to different biogeochemical forcings. To better characterize such microbial adaptations to P-deficiency in the future studies, a necessary approach is to combine biogeochemistry with micro-organisms physiology, for example by following simultaneously gene expression of phosphatase families, determining the composition of DOP along the organic matter size continuum, and measuring *in-situ* hydrolysis rates of different types of P-containing organic molecules.

1 Data Availability

The two images of sea surface temperature are distributed by CMEMS under doi 10.48670/moi-00171. Data collected by the two oceanographic cruises are available at the operational oceanographic data center Coriolis (https://www.coriolis.eu.org/Data-Products/Data-Delivery/Mediterranean-Data-selection).

Author Contribution: FV and EP: conducting the experiment, analyzing PME and PDE and writing the first manuscript. MPP, OC and AP: analyzing nutrients. VT: Providing maps and discussing mesoscale variability, MD: analysis of phytoplankton by flow cytometry, CS: analysis of heterotrophic

prokaryotes and nanoflagellates by flow cytometry, PC MPP: review and editing. All authors contributed to the article and approved the submitted version.

2 Competing interests

The authors declare that they have no conflict of interest.

3 Acknowledgments

This study is a contribution of the PERLE project, a joint initiative of the 'Chantier Méditerranée' MERMEX supported by CNRS-INSU, IFREMER, CEA, and Météo-France as part of the program MISTRALS coordinated by INSU. PERLE1 (PROTEVS cruise) was also partly managed and founded by the 'Service Hydrographique et Océanographique de la Marine' – SHOM, Brest, France (funded by the French DGA). Pigments analysis were paid by the Equipex Naos program.

We warmly thank many persons for their help on board: Frank Dumas (chief scientist of PERLE1 cruise), Florian Voron (for nanoP analysis), Sophie Guasco and Thibaut Wagener (for help in PDE PME measurements), Catherine Guigue (phospholipid data and P conversion), Paul Labatut, Barbara Marie, Eric Maria (for nutrients and DOM sampling as well as ammonium analyses), Fabrizio D'Ortenzio and Joelle Salaun (for pigments sampling). We thank the services provided by 3 platforms (SAPIG https://lov.imev-mer.fr/web/facilities/sapigh/, BioPic https://www.obs-banyuls.fr/fr/rechercher/plateformes/biopic.html, PRECYM https://precym.mio.osupytheas.fr/) for chlorophyll and flow cytometry analyses.

4 References

Aminot, A. and Kérouel, R.: Dosage automatique des nutriments dans les eaux marines, in : Méthodes d'analyses en milieu marin, edited by : IFREMER, 188 pp, 2007.

Baltar, F., Arístegui, J., Gasol, J.M., Sintes, E., van Aken, H.M., and Herndl, G.J.: High dissolved extracellular enzymatic activity in the deep central Atlantic Ocean, Aquat. Microb. Ecol., 58, 287-30, https://doi.org/10.3354/ame01377, 2010.

Ben-Ezra, T., Krom, M., D., Tsemel, A., Berman-Frank, I., Herut, B., Lehahn, Y., Rahav, E., Reich, T., Thingstad, T.F., and Sher, D.: Seasonal nutrient dynamics in the P depleted Eastern Mediterranean Sea, Deep-Sea Res. Part I, 176, article 103607, https://doi.org/10.1016/j.dsr.2021.103607, 2021.

Biller, S.J., Lundeen, R.A., Hmelo, L.R., Becker, K.W., Arellano, A.A., Dooley, K., Heal, K.R., Carlson, L.T., Van Mooy, B.A.S., Ingalls, A.E., and Chisholm, S.W.: Prochlorococcus extracellular vesicles: molecular composition and adsorption to diverse microbes, Environ. Microbiol., 24, 420-435, https://doi.org/10.1111/1462-2920.15834, 2022.

Cerdan-Garcia, E., Baylay, A., Polyviou, D., Woodward, E.M., Wrightson, L., Mahaffey, C., Lohan, M.C., Moore, C.M., Bibby, T.S., and Robidart, J.C.: Transcriptional responses of *Trichodesmium* to natural inverse gradients of Fe and P availability, ISME J., 16, 1055-1064, https://doi.org/10.1038/s41396-021-01151-1, 2021.

Christaki, U., Courties, C., Massana, R., Catala, P., Lebaron, P., Gasol, J.M. and Zubkov, M.V.: Optimized routine flow cytometric enumeration of heterotrophic flagellates using SYBR Green, Limnol. Oceanogr.: Methods, 9, 329-339, https://doi.org/10.4319/lom.2011.9.329, 2011.

Christaki, U., Van Wambeke, F. and Dolan, J. R.: Nanoflagellates (mixotrophs, heterotrophs and autotrophs) in the oligotrophic eastern Mediterranean: standing stocks, bacterivory and relationships with bacterial production, Mar. Ecol. Prog. Ser., 181, 297–307, https://doi.org/10.3354/meps181297, 1999.

Crombet, Y., Leblanc, K., Quéguiner, B., Moutin, T., Rimmelin, P., Ras, J., Claustre, H., Leblond, N., Oriol, L., and Pujo-Pay, M.: Deep silicon maxima in the stratified oligotrophic Mediterranean Sea, Biogeosciences, 8, 459–475, https://doi.org/10.5194/bg-8-459-2011, 2011.

Davis, C.E. and Mahaffey, C.: Elevated alkaline phosphatase activity in a phosphate-replete environment: Influence of sinking particles, Limnol. Oceanogr., 62, 2389-2403, https://doi.org/10.1002/lno.10572, 2017.

Djaoudi, K., Van Wambeke, F., Barani, A., Hélias-Nunige, S., Sempéré, R., and Pulido-Villena, E.: Atmospheric fluxes of soluble organic C, N, and P to the Mediterranean Sea: Potential biogeochemical implications in the surface layer, Mermex special issue, Prog. Oceanogr., 163, 59-69, https://doi.org/10.1016/j.pocean.2017.07.008, 2018a.

Djaoudi, K., Van Wambeke, F., Coppola, L., D'Ortenzio, F., Helias-Nunige, S., Raimbault, P., Taillandier, V., Testor, P., Wagener, T., and Pulido-Villena, E.: Sensitive Determination of the Dissolved Phosphate Pool for an Improved Resolution of Its Vertical Variability in the Surface Layer: New Views in the P-Depleted Mediterranean Sea, Front. Mar. Sci., 5, 234, https://doi.org/10.3389/fmars.2018.00234, 2018b.

D'Ortenzio, F., Iudicone, D., de Boyer Montegut, C., Testor, P., Antoine, D., Marullo, S., Santoleri, R., and Madec, G.: Seasonal variability of the mixed layer depth in the Mediterranean Sea as derived from in situ profile, Geophys. Res. Lett., 32, 1–4, https://doi.org/10.1029/2005GL022463, 2005.

Duhamel, S., Bjorkman, K.M., Van Wambeke, F., Moutin, T., and Karl, D.: Characterization of alkaline phosphatase activity in the North and South Pacific Subtropical Gyres: Implications for phosphorus cycling, Limnol. Oceanogr., 56, 1244-1254, https://doi.org/10.4319/lo.2011.56.4.1244, 2011.

Duhamel, S., Diaz, J.M., Adams, J.C., Djaoudi, K., Steck, V., and Waggoner, E.M.: Phosphorus as an integral component of global marine biogeochemistry, Nat. Geosci., 14, 359-368, https://doi.org/10.1038/s41561-021-00755-8, 2021.

Dunlap, P.V. and Callahan, S.M.: Characterization of a Periplasmic 3':5'-Cyclic Nucleotide Phosphodiesterase Gene, cpdP, from the Marine Symbiotic Bacterium *Vibrio fischeri*, J. Bact. 175, 4615-4624, https://doi.org/10.1128/jb.175.15.4615-4624.1993, 1993.

Dupont, C.L., Rusch, D.B., Yooseph, S., Lombardo, M.-J., Richter, R.A., Valas, R., Novotny, M., Yee-Greenbaum, J., Selengut, J.D., Haft, D.H., Halpern, A.L., Lasken, R.S., Kenneth Nealson, K., Friedman, R., and Venter, J.C.: Genomes and gene expression across light and productivity gradients in eastern subtropical Pacific microbial communities, ISME J., 9, 1076-1092, https://doi.org/10.1038/ismej.2014.198, 2015.

Durrieu de Madron, X. and Mermex Group: Marine ecosystems' responses to climatic and anthropogenic forcings in the Mediterranean, Prog. Oceanogr., 91, 97-166, https://doi.org/10.1016/j.pocean.2011.02.003, 2011.

Estrada, M., Delgado, M., Blasco, D., Latasa, M., Cabello, A.M., Benítez-Barrios, V., Fraile-Nuez, E., Mozetič, P., and Vidal, M.: Phytoplankton across Tropical and Subtropical Regions of the Atlantic, Indian and Pacific Oceans, Plos One, 11, e0151699, https://doi.org/10.1371/journal.pone.0151699, 2016.

Feuillade, M. and Dorioz, M.: Enzymatic release of phosphate in sediment of various origins, Water Res., 9, 1195-1201, 1992.

Filella, A., Riemann, L., Van Wambeke, F., Pulido-Villena, E., Vogts, A., Bonnet, S., Grosso, O., Diaz, J.M., Duhamel, S., and Benavides, M.: Contrasting Roles of DOP as a Source of Phosphorus and Energy for Marine Diazotrophs, Front. Mar. Sci. 9:923765, https://doi.org/10.3389/fmars.2022.923765, 2022.

Goutx, M., Guigue, C., Aritio, D., Ghiglione, J.-F., Pujo-Pay, M., Raybaud, V., Duflos, M., and Andersen, V.: Short term summer to autumn variability of dissolved lipid classes in the Ligurian sea (NW Mediterranean), Biogeosciences, 6, 1229–1246, https://doi.org/10.5194/bg-6-1229-2009, 2009.

Hashihama, F., Kinouchi, S., Suwa, S., Suzumura, M., and Kanda, J.: Sensitive determination of enzymatically labile dissolved organic phosphorus and its vertical profiles in the oligotrophic western North Pacific and East China Sea, J. Oceanogr., 69, 357-367, https://doi.org/10.1007/s10872-013-0178-4, 2013.

Hoppe, H.-G.: Significance of exoenzymatic activities in the ecology of brackish water: measurements by means of methylumbelliferyl-substrates, Mar. Ecol. Prog. Ser., 11, 299-308, 1983.

Hoppe, H-G. and Ullrich, S.: Profiles of ectoenzymes in the Indian Ocean: phenomena of phosphatase activity in the mesopelagic zone, Aquat. Microb. Ecol. 19: 139-148, https://doi.org/10.3354/ame019139, 1999.

Horii, S., Takahashi, K., Shiozaki, T., Takeda, S., Sato, M., Yamaguchi, T., Takine, S., Hashihama, F., Kondo, Y., Takemura, T., and Furuya, K.: East-West Variabilities of N_2 Fixation Activity in the Subtropical North Pacific Ocean in Summer: Potential Field Evidence of the Phosphorus and Iron Co-Limitation in the Western Area, JGR Oceans, 128, e2022JC019249, https://doi.org/10.1029/2022JC019249, 2023.

Huang, K., Wang, Z., Tan, J., Wang, D., Dai, X., Cen, J., Ou, L., and Lu, S.: Phosphomonoesterase and phosphodiesterase activities and their regulation during dinoflagellate blooms under different external phosphate conditions, Mar. Ecol. Prog. Ser., 698, 41-54, https://doi.org/10.3354/meps14158**,** 2022.

Huang, K., Zhuang, Y., Wang, Z., Ou, L., Cen, J., Lu, S., and Qi, Y.: Bioavailability of Organic Phosphorus Compounds to the Harmful Dinoflagellate Karenia mikimotoi, Microorganisms, 9, 1961, https://doi.org/10.3390/microorganisms9091961, 2021.

Jørgensen, C., Inglett, K.S., Jensen, H.S., Reitzel, K., and Reddy, K.R.: Characterization of biogenic phosphorus in outflow water from constructed wetlands, Geoderma, 257–258, 58–66, https://doi.org/10.1016/j.geoderma.2015.01.019, 2015.

Karl, D.L.: Microbially Mediated Transformations of Phosphorus in the Sea: New Views of an Old Cycle, Annu. Rev. Mar. Sci. 6, 279-337, https://doi.org/10.1146/annurev-marine-010213-135046, 2014.

Karl, D.M., and Björkman, K.M.: Dynamics of Dissolved Organic Phosphorus. In: Hansell D.A., and Carlson, C.A. (eds.) Biogeochemistry of Marine Dissolved Organic Matter, pp. 233-334. Burlington: Academic Press, 2015

Kiørboe, T., Ploug, H., and Thygesen, U.H.: Fluid motion and solute distribution around sinking aggregates. I. Small-scale fluxes and heterogeneity of nutrients in the pelagic environment. Mar. Ecol. Prog. Ser 211, 1-13, https://doi.org/ 10.3354/meps211001, 2001.

Kolowith, L.K., Ingall, E.D., and Benner, R.: Composition and cycling of marine organic phosphorus, Limnol. Oceanogr., 46, 309-320, https://doi.org/10.4319/lo.2001.46.2.0309, 2001.

Labry, C., Delmas, D., and Herbland, A.: Phytoplankton and bacterial alkaline phosphatase activities in relation to phosphate and DOP availability within the Gironde plume waters (Bay of Biscay), J. Exp. Mar. Biol. Ecol., 318, 213-225, https://doi.org/10.1016/j.jembe.2004.12.017, 2005.

Labry, C., Delmas, D., Youenou, A., Quere, J., Leynaert, L., Fraisse, S., Raimonet, M., and Ragueneau, O.: High alkaline phosphatase activity in phosphate replete waters: The case of two macrotidal estuaries, Limnol. Oceanogr., 61, 1513-1529, https://doi.org/10.1002/lno.10315, 2016.

Lidbury, I.D., Scanlan, D.J., Murphy, A.R., Christie-Oleza, J.A., Aguilo-Ferretjans, M.M., Hitchcock, A., and Daniell, T.J.: A widely distributed phosphate-insensitive phosphatase presents a route for rapid organophosphorus remineralization in the biosphere, Proc. Natl. Acad. Sci., 119, article e2118122119, https://doi.org/10.1073/pnas.2118122119, 2022.

Lomas, M. W., Burke, A. L., Lomas, D. A., Bell, D. W., Shen, C., Dyhrman, S. T., and Ammerman, J.W.: Sargasso Sea phosphorus biogeo chemistry: an important role for dissolved organic phosphorus (DOP), Biogeosciences, 7, 695–710. https://doi.org/10.5194/bg-7-695-2010, 2010.

Luo, H., Benner, R., Long, R.A., and Hu, J.: Subcellular localization of marine bacterial alkaline phosphatases, Proc. Natl. Acad. Sci., 106, 21219-21223, https://doi.org/10.1073/pnas.0907586106, 2009.

Mahaffey, C., Reynolds, S., Davis, C.E., and Lohan, M.C.: Alkaline phosphatase activity in the subtropical ocean: insights from nutrient, dust and trace metal addition experiments, Front. Mar. Sci., 1, article 73. https://doi.org/10.3389/fmars.2014.00073, 2014.

Marie, D., Partenski, F., Jaquet, S., and Vaulot, D.: Enumeration and cell cycle analysis of natural population of marine picoplankton by flow cytometry using the nucleic acid stain SYBR green I, Appl. Environ. Microbiol. 6, 186-193, 1997.

Marie, D., Simon, N., Guillou, L., Partensky, F., and Vaulot, D.: Flow Cytometry Analysis of Marine Picoplankton, in Living Color: Protocols in Flow Cytometry and Cell Sorting, edited by: Diamond R. A. and Demaggio S., Springer, Berlin, 421–454, eBook ISBN 978-3-642-57049-0, 2000.

Mella-Flores, D., Mazard, S., Humily, F., Partensky, F., Mahé, F., Bariat, L., Courties, C., Marie, D., Ras, J., Mauriac, R., Jeanthon, C., Mahdi Bendif, E., Ostrowski, M., Scanlan, D.J., and Garczarek, L.: Is the distribution of Prochlorococcus and Synechococcus ecotypes in the Mediterranean Sea affected by global warming? Biogeosciences 8, 2785–2804, https://doi.org/10.5194/bg-8-2785-2011, 2011.

Monbet, P., McKelvie, I.D., Saefumillah, A., and Worsfold, P.J.: A Protocol to Assess the Enzymatic Release of Dissolved Organic Phosphorus Species in Waters under Environmentally Relevant Conditions, Environ. Sci. Technol., 41, 7479-7485. https://doi.org/10.1021/es070573c, 2007.

Monbet, P., McKelvie, I.D., and Worsfold, P.J.: Dissolved organic phoshorus speciation in the waters of the Tamar Estuary (SW England). Geochim. Cosmochim. Acta, 73, 1027-1038, https://doi.org/10.1016/j.gca.2008.11.024, 2009.

Moutin, T., Karl, D. M., Duhamel, S., Rimmelin, P., Raimbault, P., Van Mooy, B. A. S., and Claustre, H.: Phosphate availability and the ultimate control of new nitrogen input by nitrogen fixation in the tropical Pacific Ocean, Biogeosciences, 5, 95–109, https://doi.org/10.5194/bg-5-95-2008, 2008.

Muscarella, M.E., Bird, K.C., Larsen, M.L., Placella, S.A., and Lennon, J.T.: Phosphorus resource heterogeneity in microbial food webs, Aquat. Microb. Ecol., 73: 259-272, https://doi.org/10.3354/ame01722, 2014.

Nagata, T., and Kirchman, D.L.: Release of dissolved organic matter by heterotrophic protozoa: implications for the microbial food webs. Arch. Hydrobiol. Beih. Ergebn. Limnol. 35, 99-109, 1992.

Noskova, Y., Likhatskaya, G., Terentieva, N., Son, O., Tekutyeva, L., and Balabanova, L.: A Novel Alkaline Phosphatase/Phosphodiesterase, CamPhoD, from Marine Bacterium Cobetia amphilecti KMM 296, Mar. Drugs, 17, article 657, https://doi.org/10.3390/md17120657, 2019.

Pujo-Pay, M., Conan, P., and Raimbault, P.: Excretion of dissolved organic nitrogen by phytoplankton assessed by wet oxidation and N-15 tracer procedures, Mar. Ecol. Prog. Ser., 153, 99-111, https://doi.org/10.3354/meps153099, 1997.

Pujo-Pay, M. and Raimbault, P.: Improvements of the wet-oxidation procedure for simultaneous determination of particulate organic nitrogen and phosphorus collected on filters, Mar. Ecol. Prog. Ser., 105, 203-207, 1994.

Pujo-Pay, M., Conan, P., Oriol, L., Cornet-Barthaux, V., Falco, C., Ghiglione, J.-F., Goyet, C., Moutin, T., and Prieur, L.: Integrated survey of elemental stoichiometry (C, N, P) from the western to eastern Mediterranean Sea, Biogeosciences, 8, 883–899, https://doi.org/10.5194/bg-8-883-2011, 2011.

Powley, H.T., Van Cappellen, P., and Krom M.D.: Nutrient Cycling in the Mediterranean Sea: The Key to Understanding How the Unique Marine Ecosystem Functions and Responds to Anthropogenic Pressures, In Mediterranean Identities - Environment, Society, Culture, edited by Furest-Bjelis B. Intech, 47-77, 2017.

Pulido-Villena, E., Desboeufs, K. Djaoudi, K., Van Wambeke, F., Barrillon, S., Doglioli, A., Petrenko, A. Taillandier, V., Fu, F., Gaillard, T., Guasco, S., Nunige, S., Triquet, S., and Guieu, C.: Phosphorus cycling in the upper waters of the Mediterranean Sea (PEACETIME cruise): relative contribution of external and internal sources, Biogeosciences, 18, 5871-7889. doi:10.5194/bg-18-5871-2021, 2021.

Rahav, E., Herut, B., Levi, A., Mulholland, M., and Berman-Frank, I.: Springtime contribution of dinitrogen fixation to primary production across the Mediterranean Sea. Ocean Sci. 0, 489-498, https://doi.org/10.5194/os-9-489-2013, 2013.

Ras, J., Claustre, H., and Uitz, J.: Spatial variability of phytoplankton pigment distributions in the Subtropical South Pacific Ocean: comparison between in situ and predicted data, Biogeosciences, 5, 353–369, https://doi.org/10.5194/bg-5-353-2008, 2008.

Reich, T., Ben-Ezra, T., Belkin, N., Aharonovich, D., Roth-Rosenberg, D., Givati, S., Bialik, M., Herut, B., Berman-Frank, I., Frada, M., Krom, M., D., Lehahn, Y., Rahav, E., and Sherr, D.: A year in the life of the Eastern

Mediterranean: Monthly dynamics of phytoplankton and bacterioplankton in an ultra-oligotrophic sea. Deep-Sea Res. I 182, article 103720, https://doi.org/10.1016/j.dsr.2022.103720, 2022.

Sala, M.M., Karner, M., Arin, L., and Marrassé, C.: Measurement of ectoenzyme activities as an indication of inorganic nutrient imbalance in microbial communities, Aquat. Microb. Ecol., 23, 301-311, 2001.

Sato, M., Sakuraba, R., and Hashihama, F.: Phosphate monoesterase and diesterase activities in the North and South Pacific Ocean, Biogeosciences, 10, 7677–7688, https://doi.org/10.5194/bg-10-7677-2013, 2013.

Scharek, R. and Latasa, M.: Growth, grazing and carbon flux of high and low nucleic acid bacteria differ in surface and deep chlorophyll maximum layers in the NW Mediterranean Sea, Aquat. Microb. Ecol., 46, 153-161, 2007.

Sisma-Ventura, G. and Rahav, E.: DOP Stimulates Heterotrophic Bacterial Production in the Oligotrophic Southeastern Mediterranean Coastal Waters, Front. Microbiol. 10, 1913, https://doi.org/10.3389/fmicb.2019.01913, 2019.

Srivastava, A., Saavedra, D.E.M., Thomson, B., García, J.A.L., Zhao, Z., Patrick, W.M., Herndl, G.J., and Baltar, F.: Enzyme promiscuity in natural environments: alkaline phosphatase in the ocean, ISME J., 15, 3375–3383, https://doi.org/10.1038/s41396-021-01013-w, 2021.

Statham, P.J., and Hart, V.: Dissolved iron in the Cretan sea (eastern Mediterranean) Limnol. Oceanogr, 50, 1142-1148, 2005.

Su, B., Song, X., Duhamel, S., Mahaffey, C., Davis, C., Ivančić, I., and Liu, J.: A data set of global ocean alkaline phosphatase activity, Sci. data, 10, 205, https://doi.org/10.1038/s41597-023-02081-7, 2023.

Suzumura, M., Hashihama, F., Yamada, N., and Kinouchi, S.: Dissolved phosphorus pools and alkaline phosphatase activity in the euphotic zone of the western North Pacific Ocean, Front. Microbiol., 3, article 99, https://doi.org/10.3389/fmicb.2012.00099, 2012.

Suzumura, M. and Ingall, E.D.: Concentrations of lipid phosphorus and its abundance in dissolved and particulate organic phosphorus in coastal seawater, Mar. Chem., 75, 141-149, https://doi.org/10.1016/S0304-4203(01)00034-2, 2001.

Suzumura, M., Ishikawa, K., and Ogawa, H.: Characterization of dissolved organic phosphorus in coastal seawater using ultrafiltration and phosphohydrolytic enzymes, Limnol. Oceanogr., 43, 1553-1564, https://doi.org/10.4319/lo.1998.43.7.1553, 1998.

Taillandier , V., D'Ortenzio , F., Prieur , L., Conan , P., Coppola , C., Cornec , M., Dumas, F., Durrieu de Madron , X., Fach , B., Fourrier , M., Gentil, M., Hayes , D., Husrevoglu , H., Legoff, H., Le Ster, L., Örek, H., Ozer, T., Poulain, P.M., Pujo-Pay, M., Ribera d'Alcalà, M., Salihoglu, B., Testor , P., Velaoras , D., Wagener, T., and Wimart-Rousseau, C.: Sources of the Levantine Intermediate Water in Winter 2019, J. Geophys. Res. Oceans, 27, e2021JC017506, https://doi.org/10.1029/2021JC017506, 2022.

Tanaka, T., Thingstad, T. F., Christaki, U., Colombet, J., Cornet-Barthaux, V., Courties, C., Grattepanche, J.-D., Lagaria, A., Nedoma, J., Oriol, L., Psarra, S., Pujo-Pay, M., and Van Wambeke, F.: Lack of P-limitation of

phytoplankton and heterotrophic prokaryotes in surface waters of three anticyclonic eddies in the stratified Mediterranean Sea, Biogeosciences, 8, 525–538, https://doi.org/10.5194/bg-8-525-2011, 2011.

Thingstad, T. F., Krom, M. D., Mantoura, R. F. C., Flaten, G. A. F., Groom, S., Herut, B., Kress, N., Law, C. S., Pasternak, A., Pitta, P., Psarra, S., Rassoulzadegan, F., Tanaka, T., Tselepides, A., Wassmann, P., Woodward, E. M. S., Wexels Riser, C., Zodiatis, G., and Zohary, T.: Nature of Phosphorus Limitation in the Ultra-oligotrophic Eastern Mediterranean, Science, 309, 1068–1071, https://doi.org/10.1126/science.1112632, 2005.

Thomson, B., Wenley, J., Lockwood, S., Twigg, I., Currie, K., Herndl, G., Hepburn, C.D., and Baltar, F.: Relative Importance of Phosphodiesterase vs. Phosphomonoesterase (Alkaline Phosphatase) Activities for Dissolved Organic Phosphorus Hydrolysis in Epi and Mesopelagic Waters, Front. Earth Sci., 8, article 560893, https://doi.org/10.3389/feart.2020.560893, 2020.

Turner, B.J., McKelvie, I.D., and Haygarth, P.M.: Characterization of water-extractable soil organic phosphorus by phosphatase hydrolysis, Soil Biol. Biogeochem., 34, 27-35, https://doi.org/10.1016/S0038-0717(01)00144-4, 2002.

Urvoy, M., Labry, C., Delmas, D., Layla, C. and L'Helguen, S.: Microbial enzymatic assays in environmental water samples: impact of Inner Filter Effect and substrate concentrations. Limnology and Oceanography: Methods 18, 725-738. https://doi.org/10.1002/lom3.10398, 2020.

Van Wambeke, F., Christaki, U., Giannakourou, A., Moutin, T., and Souvemerzoglou, K.: Longitudinal and vertical trends of bacterial limitation by phosphorus and carbon in the Mediterranean Sea. Microb. Ecol., 43, 119-133, https://doi.org/10.1007/s00248-001-0038-4, 2002.

Van Wambeke, F., Taillandier, V., Desboeufs, K., Pulido-Villena, E., Dinasquet, J., Engel, A., Marañón, E., Ridame, C., and Guieu, C.: Influence of atmospheric deposition on biogeochemical cycles in an oligotrophic ocean system. Biogeosciences, 15, 5699–5717, https://doi.org/10.5194/bg-18-5699-2021, 2021.

Van Wambeke, F., Taillandier, V,, De Madron, X., Conan, P., Pujo-Pay, M., Psarra, S., Rabouille, S., Crispi, O., Baumas, C., and Pulido-Villena, E.: Mesoscale variability of phosphorus stocks and biogeochemical fluxes in the mixed layer during 2 contrasted seasons in the Eastern Mediterranean Sea', in prep.

Van Wambeke, F., Gimenez, A., Duhamel, S., Dupouy, C., Lefevre, D., Pujo-Pay, M. and Moutin, T.: Dynamics and controls of heterotrophic prokaryotic production in the western tropical South Pacific Ocean: links with diazotrophic and photosynthetic activity. Biogeosciences 15, 2669 – 2689, https://doi.org/10.5194/bg-15-2669-2018, 2018.

Van Wambeke, F., Christaki, U., Giannakourou, A., Moutin, T., and Souvemerzoglou, K.: Longitudinal and vertical trends of bacterial limitation by phosphorus and carbon in the Mediterranean Sea. Microbial Ecology 43, 119-133, 2002.

Yamaguchi, T., Sato, M., Hashihama , F., Ehama, M., Shiozaki, T., Takahashi, K., and Furuya, K.: Basin-Scale Variations in Labile Dissolved Phosphoric Monoesters and Diesters in the Central North Pacific Ocean, J. Geophys. Res. Oceans, 124, 3058–3072, https://doi.org/10.1029/2018JC014763, 2019.

Young, C.L., and Ingall, E.D.: Marine Dissolved Organic Phosphorus Composition: Insights from Samples Recovered Using Combined Electrodialysis/Reverse Osmosis. Aquat Geochem 16, 563-574, https://doi.org/10.1007/s10498-009-9087-y, 2010.

Zaccone, R., Boldrin, A., Caruso, G., La Ferla, R., Maimone, G., Santinelli, C., and Turchetto, M..: Enzymatic Activities and Prokaryotic Abundance in Relation to Organic Matter along a West–East Mediterranean Transect (TRANSMED Cruise), Microb. Ecol. 64, 54-66, https://doi.org/10.1007/s00248-012-0011-4, 2012.

Zhang, J.-Z., and Chi, J.: Automated analysis of nano-molar concentrations of phosphate in natural waters with liquid waveguide, Environ. Sci. Technol., 36, 1048-1053, https://doi.org/10.1021/es011094v, 2002.

Zheng, L., Ren, M., Xie, E., Ding, A., Liu, Y., Deng, S. and Zhang, D.: Roles of Phosphorus Sources in Microbial Community Assembly for the Removal of Organic Matters and Ammonia in Activated Sludge, Front. Microbiol., article 10:1023, https://doi.org/10.3389/fmicb.2019.01023, 2019.

Zohary, T. and Robarts, R. D.: Experimental study of microbial P limitation in the eastern Mediterranean, Limnol. Oceanogr., 43, 38–395, 1998.

5 Figure Legends

FIGURE 1 Map of the cruise PERLE 1 south east Crete in October 2018. Sampled stations are indicated in green dots. In background image of Sea Surface Temperature (L3S ultra-high-resolution product distributed by CMEMS) of October 16, 2018. The warm core Ierapetra anticyclone is observed around 34°30'N, 26°E.

FIGURE 2 Map of the cruise PERLE 2 surrounding Crete in February-March 2019. Sampled stations are indicated in green dots. In background image of Sea Surface Temperature (L3S ultra-high-resolution product distributed by CMEMS) of March 4, 2019. The cold core Rhodes cyclonic gyre is observed around 35°N, 29°E.

FIGURE 3 (a, b, c) Vertical distributions of dissolved inorganic phosphorus (DIP). (d, e, f) Vertical distributions of the sum of nitrate + nitrite concentrations (NOx). a, d: PERLE1 cruise (October 2018); b, e: Mixed and anticyclonic stations of PERLE2 cruise (Feb-March 2019); c, f: other stations of PERLE2 Cruise.

FIGURE 4 (a, b, c) Vertical distributions of dissolved organic phosphorus (DOP) and labile dissolved organic phosphorus (L_{DOP}). (d, e, f) Vertical distributions (0-300 m) of maximum hydrolysis rates of phosphomonoesterase (Vm PME) and phosphodiesterase (Vm PDE). a, d: PERLE1 cruise (October 2018); b, e: Mixed and anticyclonic stations of PERLE2 cruise (Feb-March 2019); c, f: other stations of PERLE2 Cruise.

FIGURE 5 (a) Example of a concentration kinetic with MUF-P addition, (b): with a focus on the 0-1 µM range. (c) Example of a concentration kinetic with bis-MUF-P addition, (d) with a focus on the 0-1 µM range.

FIGURE 6 (a, b, c) Vertical distributions of PME Km. (d, e, f) Vertical distributions PDE Km. a, d: PERLE1 cruise (October 2018); b, e: Mixed and anticyclonic stations of PERLE2 cruise (Feb-March 2019); c, f: other stations of PERLE2 Cruise.

FIGURE 7 (a) Relationships between Km PME and Km PDE versus DIP concentrations. (b) Relationships between Vm PME and Vm PDE versus DIP concentrations. Open circles: PDE, full circles: PME, red: autumn cruise (PERLE1), black: winter cruise (PERLE2).

Table 1. Position, sampling date and some physical and biogeochemical characteristics of the stations studied during PERLE2 (Feb-March 2019) and PERLE1 (October 2018) cruises. Lat: Latitude, Long: longitude, SST: Sea surface temperature, MLD: mixed layer depth, Z Pcline: phosphacline depth, Z Ncline: nitracline depth.

Cruise	Station	Date Time (h:min) utc	Lat °N	Long °E	SST °C	MLD m	Z Pcline m	Z Ncline m	Integrated Tchla mg m^{-2}
PERLE1	2	10/10/18 20:39	34.82	26.52	24.9	38	106	126	16.1
PERLE1	5	11/10/18 10:36	34.29	26.51	25.1	48	188	154	14.6
PERLE1	12	12/10/18 8:43	33.32	26.49	26.2	22	119	105	13.4
PERLE1	15	15/10/18 3:11	34.21	25.95	25.3	30	145	123	13.1
PERLE1	16	15/10/18 8:38	34.21	25.65	25.5	25	193	143	11
PERLE1	19	16/10/18 0:00	34.21	26.76	24.9	23	175	137	21.4
PERLE1	20	16/10/18 4:40	34.21	27.10	23.9	36	122	90	15
PERLE1	23	16/10/18 17:09	33.90	26.64	24.9	35	167	123	23.8
PERLE1	25	18/10/18 1:29	34.21	26.05	25.9	88	239	185	20.9
PERLE1	27	19/10/18 23:08	33.83	27.09	24.1	19	100	83	16.5
PERLE1	30	20/10/18 8:10	33.82	27.82	24.7	18	135	98	16.8
PERLE2	1	27/2/19 8:33	35.86	25.30	16.0	145	82	60	51.7
PERLE2	13	28/2/19 17:01	35.62	23.54	15.8	118	247	188	59.2
PERLE2	15	1/3/19 1:44	35.95	23.76	15.6	269	164	90	66.2
PERLE2	21	2/3/19 3:22	34.44	22.82	15.5	27	115	17	33.2
PERLE2	26	2/3/19 22:30	34.44	23.73	15.6	113	94	70	39.8
PERLE2	35	4/3/19 2:27	34.33	24.52	15.6	53	164	144	52.6
PERLE2	44	5/3/19 3:49	33.62	24.38	15.7	61	67	24	28.2
PERLE2	50	6/3/19 2:10	34.32	25.30	16.6	213	258	211	69.3
PERLE2	58	7/3/19 5:23	34.29	26.09	16.0	97	151	101	60.9
PERLE2	68	8/3/19 20:50	33.59	28.81	16.4	34	89	40	40.3
PERLE2	75	10/3/19 1:10	33.86	27.99	16.7	45	73	11	48.1
PERLE2	80	10/3/19 15:40	33.96	27.32	16.4	14	37	2	65.6
PERLE2	90	12/3/19 1:03	34.68	26.90	16.6	25	82	64	45.6
PERLE2	94	12/3/19 13:03	34.94	26.74	16.8	19	15	0	26.5
PERLE2	104	13/3/19 6:32	35.37	26.66	17.4	63	177	134	39.5
PERLE2	108	13/3/19 17:14	35.84	27.43	17.4	103	265	240	67.4
PERLE2	111	14/3/19 13:29	33.96	27.32	16.1	53	45	32	63.8
PERLE2	116	15/3/19 2:56	34.68	26.90	16.2	48	104	5	38.9

Table 2. Mean abundances of main flow cytometric groups and nutrient concentrations inside ML at each station. Hprok heterotrophic prokaryotes, Proc: *Prochlorococcus*, Syn: *Synechococcus*, Picoeuk: Nanophytoeukaryotes, Nanoeuk: Nanophytoeukaryotes, DIP: dissolved inorganic phosphorus, NOx: sum nitrate+nitrite, DOP: dissolved organic phosphorus, L_{DOP}: labile dissolved organic phosphorus, and the NOx:DIP ratio.na: not available.

		x 10^5 ml^{-1}	x 10^3 ml^{-1}	x 10^3 ml^{-1}	x 10^3 ml^{-1}	ml^{-1}	nM	µM	nM	nM	%	ratio
Cruise	station	Hprok	Proc	Syn	Picoeuk	Nanoeuk	DIP	NOx	DOP	L_{DOP}	L_{DOP}	Nox :DIP
PERLE1	2	3	0.87	13.1	0.42	90	13	0.011	21	4	19	0.8
PERLE1	5	3.2	0.57	11.3	0.4	117	9	0.012	19	6	34	1.3
PERLE1	12	3.1	0.11	6	0.29	64	10	0.01	16	7	46	0.9
PERLE1	15	3.8	0.59	13.6	0.62	125	12	0.026	18	2	11	2.3
PERLE1	16	3.9	0.48	10.3	0.37	56	10	0.01	40	na	na	1
PERLE1	19	3.2	0.62	11.1	0.42	54	12	0.035	21	3	16	2.9
PERLE1	20	3.8	3.1	14	0.62	73	8	0.01	36	6	17	1.3
PERLE1	23	3.6	0.68	11.9	0.58	105	12	0.012	47	5	10	1
PERLE1	25	3.1	0.49	13.1	0.55	83	8	0.011	18	8	46	1.4
PERLE1	27	3.4	2.6	11.5	0.48	84	16	0.024	22	6	28	1.5
PERLE1	30	2.7	0.32	8.3	0.39	52	8	0.019	22	10	46	2.5
PERLE2	1	3	0.38	0.35	0.09	13	24	0.99	69	31	44	41
PERLE2	13	3.6	0.87	0.86	0.07	15	20	1.13	62	37	59	56
PERLE2	15	3.9	0.9	0.71	0.24	13	24	1.13	74	11	15	48
PERLE2	50	4.2	1.2	1.8	0.06	14	8	0.5	71	9	14	58
PERLE2	104	3.9	1.2	2.9	0.17	28	9	0.45	26	16	61	50
PERLE2	108	4.1	0.68	1.9	0.09	25	7	0.44	22	13	44	59
PERLE2	21	3.4	1.8	2.3	0.06	20	12	0.17	44	5	12	14
PERLE2	26	4.4	2.1	2.2	0.06	21	10	0.8	49	9	18	78
PERLE2	35	3.3	1.7	2.4	0.08	25	10	0.32	62	7	13	31
PERLE2	44	3.2	2	1.9	0.07	14	9	0.7	56	14	25	74
PERLE2	58	na	1.7	1.9	0.24	43	11	0.96	39	12	31	87
PERLE2	68	3.6	4.3	3.1	0.22	46	9	0.43	34	11	31	46
PERLE2	75	2.9	1.1	2.8	0.06	27	5	0.22	56	29	65	41
PERLE2	80	6.1	1.7	3.8	0.27	48	11	0.034	47	12	26	3
PERLE2	90	4.5	3.4	5.4	0.17	49	9	0.22	55	16	29	25
PERLE2	94	6.1	3.1	5.9	0.3	31	7	0.34	57	19	33	45
PERLE2	111	7.1	5.1	4.6	0.26	22	11	0.79	42	15	38	70
PERLE2	116	6.6	2.9	3.6	0.19	23	8	0.61	25	13	54	76

Table 3. Mean PME and PDE kinetic parameters (Km, Vm), and specific Vm activities inside ML at each station. For cell specific activity, Vm rates are divided by the abundance of Hprok cells, for biomass specific Vm, Vm rates are divided by the sum of phytoplankton carbon biomass + Hprok carbon biomass. na: not available.

		Vm		Km		cell specific Vm		biomass specific Vm	
		nmol l^{-1} h^{-1}		µM		x 10^{-18} mol $cell^{-1}$ h^{-1}		nmol µg C^{-1} h^{-1}	
Cruise	Station	PME	PDE	PME	PDE	PME	PDE	PME	PDE
PERLE1	2	2.41	2.18	0.062	2.77	7.9	7.23	0.350	0.311
PERLE1	5	1.49	1.55	0.060	2.25	5.1	5.30	0.227	0.236
PERLE1	12	1.78	4.76	0.083	7.58	6.0	16.13	0.304	0.815
PERLE1	15	2.38	4.00	0.062	4.14	6.2	10.48	0.310	0.521
PERLE1	16	2.21	1.66	0.068	1.66	5.7	4.25	0.280	0.211
PERLE1	19	2.68	4.16	0.068	4.44	8.3	12.88	0.356	0.553
PERLE1	20	1.88	1.30	0.059	1.23	4.9	3.42	0.221	0.158
PERLE1	23	2.58	3.70	0.068	4.03	7.3	10.46	0.311	0.456
PERLE1	25	2.40	4.23	0.054	4.86	7.6	12.84	0.314	0.539
PERLE1	27	2.71	1.87	0.075	1.59	7.9	5.45	0.378	0.261
PERLE1	30	2.05	2.78	0.065	3.42	7.4	10.04	0.344	0.467
PERLE2	1	0.41	0.26	0.151	1.62	1.4	0.83	0.023	0.014
PERLE2	13	0.37	0.54	0.185	1.92	1.0	1.49	0.018	0.026
PERLE2	15	0.22	0.14	0.209	1.25	0.6	0.36	0.013	0.008
PERLE2	50	1.45	3.24	0.106	3.14	3.6	8.02	0.083	0.186
PERLE2	104	4.11	8.54	0.134	7.05	10.7	21.93	0.187	0.392
PERLE2	108	4.81	7.29	0.216	6.54	11.6	17.55	0.180	0.273
PERLE2	21	2.61	3.10	0.118	1.76	7.7	9.14	0.139	0.165
PERLE2	26	1.62	1.11	0.093	1.10	3.7	2.57	0.083	0.059
PERLE2	35	3.42	7.91	0.115	4.20	10.7	24.78	0.194	0.448
PERLE2	44	1.81	4.16	0.106	4.46	5.6	12.87	0.117	0.269
PERLE2	58	2.84	4.50	0.136	4.73	na	na	na	na
PERLE2	68	7.57	11.89	0.170	6.42	21.7	34.20	0.581	0.910
PERLE2	75	4.10	8.72	0.110	4.31	14.3	30.38	0.253	0.537
PERLE2	80	18.87	22.02	0.288	7.24	30.7	35.80	0.356	0.415
PERLE2	90	14.53	20.77	0.260	6.63	31.9	45.36	0.539	0.772
PERLE2	94	10.89	18.60	0.239	6.97	17.8	30.46	0.344	0.588
PERLE2	111	4.66	6.71	0.241	6.61	6.6	9.46	0.134	0.193
PERLE2	116	6.00	7.35	0.168	6.23	9.1	11.18	0.219	0.268

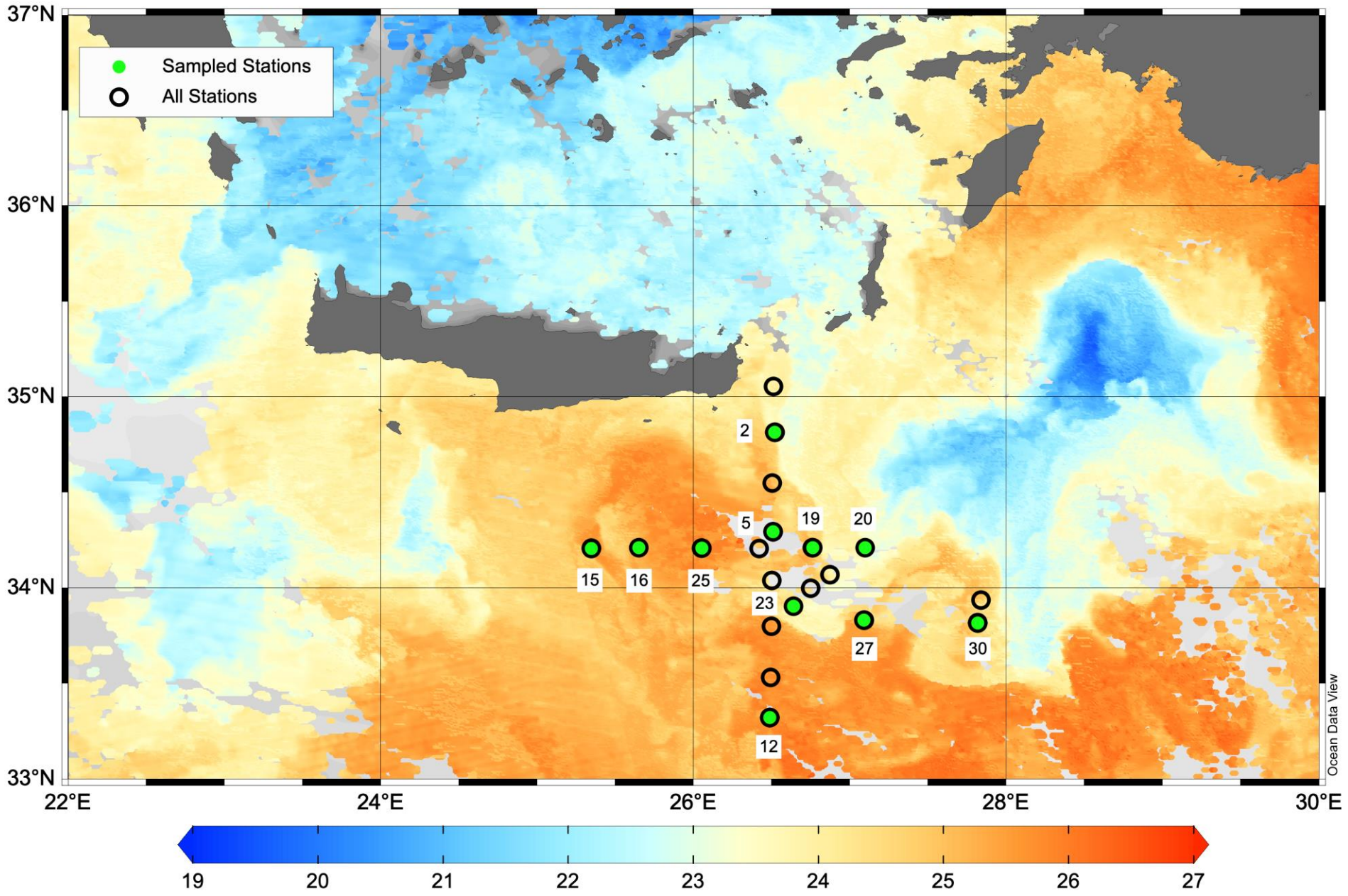
Sampled Stations
All Stations
37°N
36°N
35°N
34°N
33°N
22°E
24°E
26°E
28°E
30°E
2
5
19
20
15
16
25
23
27
30
12
19
20
21
22
23
24
25
26
27
Ocean Data View

Fig 1

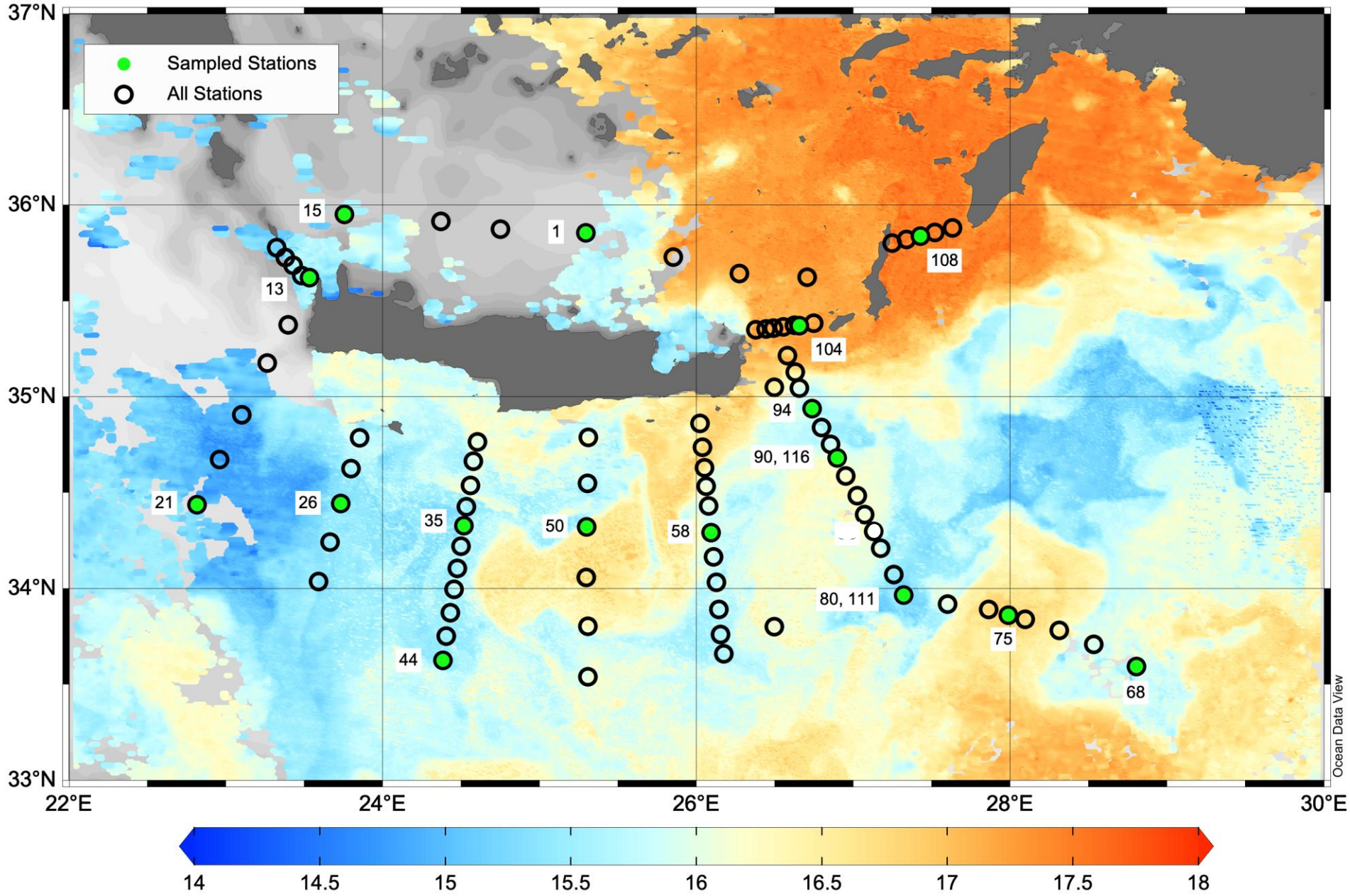
Sampled Stations
All Stations
37°N
36°N
35°N
34°N
33°N
22°E
24°E
26°E
28°E
30°E
15
1
13
108
104
94
90, 116
21
26
35
50
58
80, 111
75
44
68
14
14.5
15
15.5
16
16.5
17
17.5
18
Ocean Data View

Fig 2

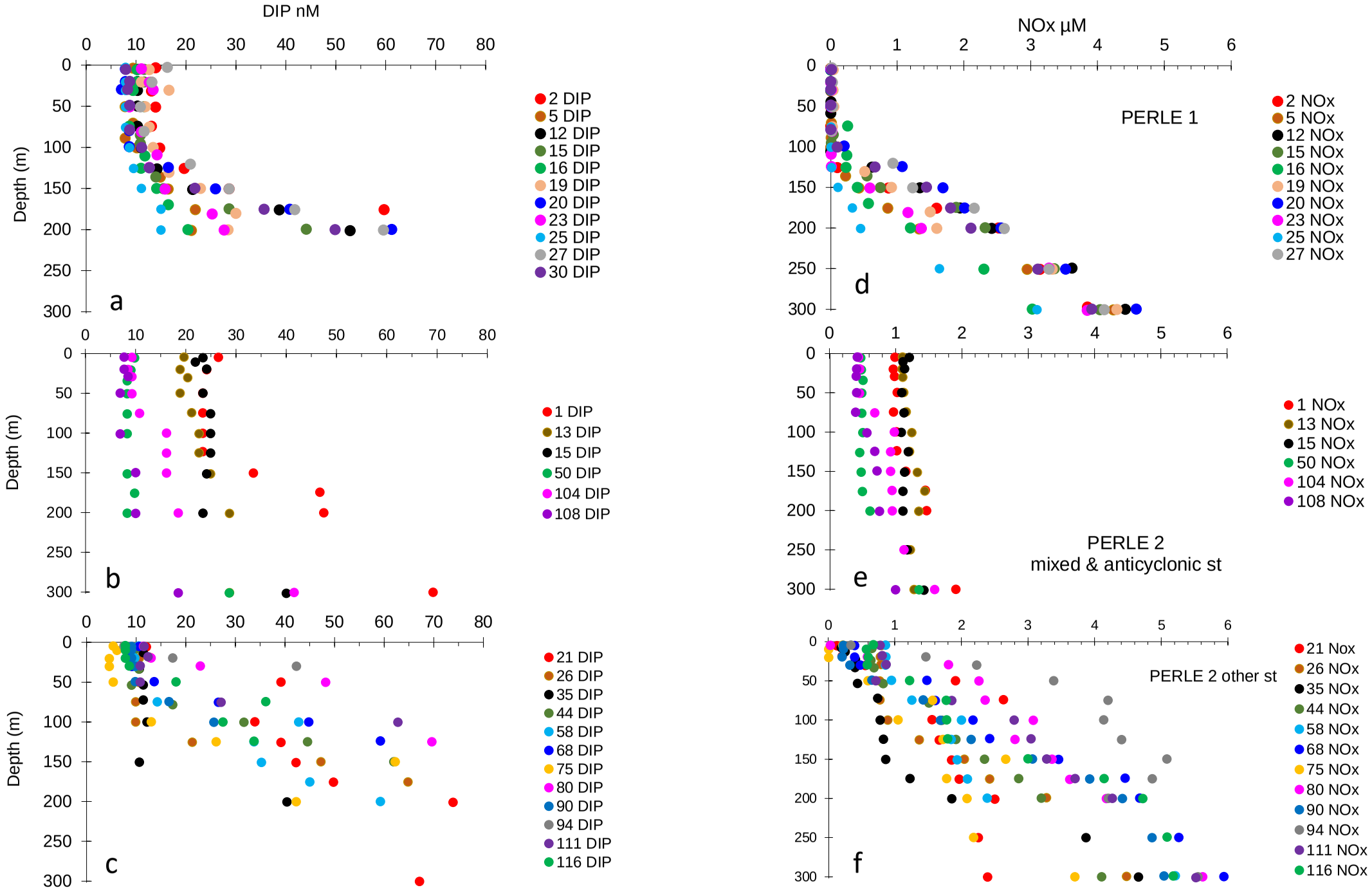
DIP nM
Depth (m)
a
2 DIP
5 DIP
12 DIP
15 DIP
16 DIP
19 DIP
20 DIP
23 DIP
25 DIP
27 DIP
30 DIP
b
1 DIP
13 DIP
15 DIP
50 DIP
104 DIP
108 DIP
c
21 DIP
26 DIP
35 DIP
44 DIP
58 DIP
68 DIP
75 DIP
80 DIP
90 DIP
94 DIP
111 DIP
116 DIP
NOx µM
PERLE 1
d
2 NOx
5 NOx
12 NOx
15 NOx
16 NOx
19 NOx
20 NOx
23 NOx
25 NOx
27 NOx
e
1 NOx
13 NOx
15 NOx
50 NOx
104 NOx
108 NOx
PERLE 2
mixed & anticyclonic st
f
PERLE 2 other st
21 Nox
26 NOx
35 NOx
44 NOx
58 NOx
68 NOx
75 NOx
80 NOx
90 NOx
94 NOx
111 NOx
116 NOx

Fig 3

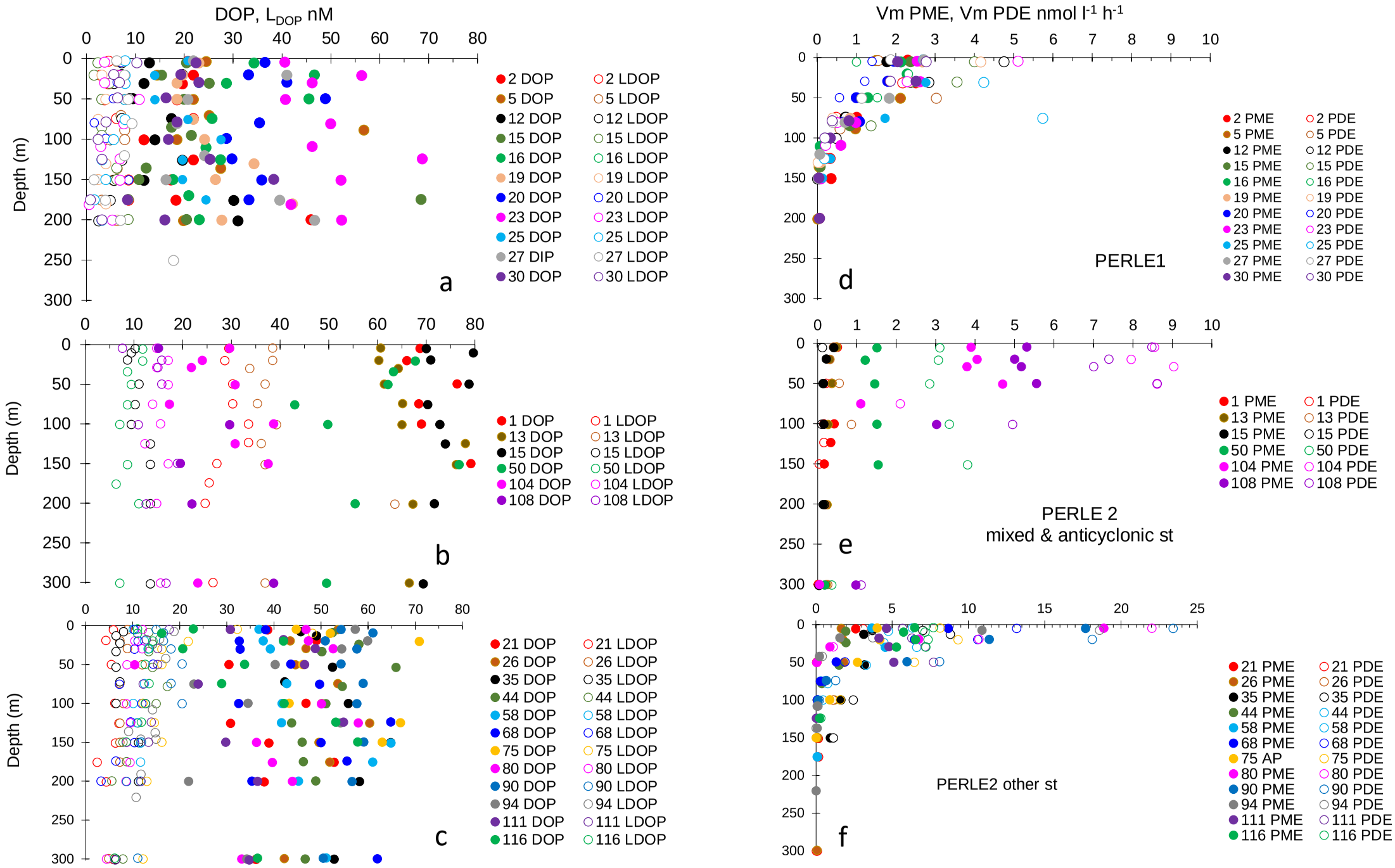
DOP, L_{DOP} nM
Depth (m)
a
2 DOP
5 DOP
12 DOP
15 DOP
16 DOP
19 DOP
20 DOP
23 DOP
25 DOP
27 DIP
30 DOP
2 LDOP
5 LDOP
12 LDOP
15 LDOP
16 LDOP
19 LDOP
20 LDOP
23 LDOP
25 LDOP
27 LDOP
30 LDOP
b
1 DOP
13 DOP
15 DOP
50 DOP
104 DOP
108 DOP
1 LDOP
13 LDOP
15 LDOP
50 LDOP
104 LDOP
108 LDOP
c
21 DOP
26 DOP
35 DOP
44 DOP
58 DOP
68 DOP
75 DOP
80 DOP
90 DOP
94 DOP
111 DOP
116 DOP
21 LDOP
26 LDOP
35 LDOP
44 LDOP
58 LDOP
68 LDOP
75 LDOP
80 LDOP
90 LDOP
94 LDOP
111 LDOP
116 LDOP
Vm PME, Vm PDE nmol l^{-1} h^{-1}
d
PERLE1
2 PME
5 PME
12 PME
15 PME
16 PME
19 PME
20 PME
23 PME
25 PME
27 PME
30 PME
2 PDE
5 PDE
12 PDE
15 PDE
16 PDE
19 PDE
20 PDE
23 PDE
25 PDE
27 PDE
30 PDE
e
PERLE 2
mixed & anticyclonic st
1 PME
13 PME
15 PME
50 PME
104 PME
108 PME
1 PDE
13 PDE
15 PDE
50 PDE
104 PDE
108 PDE
f
PERLE2 other st
21 PME
26 PME
35 PME
44 PME
58 PME
68 PME
75 AP
80 PME
90 PME
94 PME
111 PME
116 PME
21 PDE
26 PDE
35 PDE
44 PDE
58 PDE
68 PDE
75 PDE
80 PDE
90 PDE
94 PDE
111 PDE
116 PDE

Fig 4

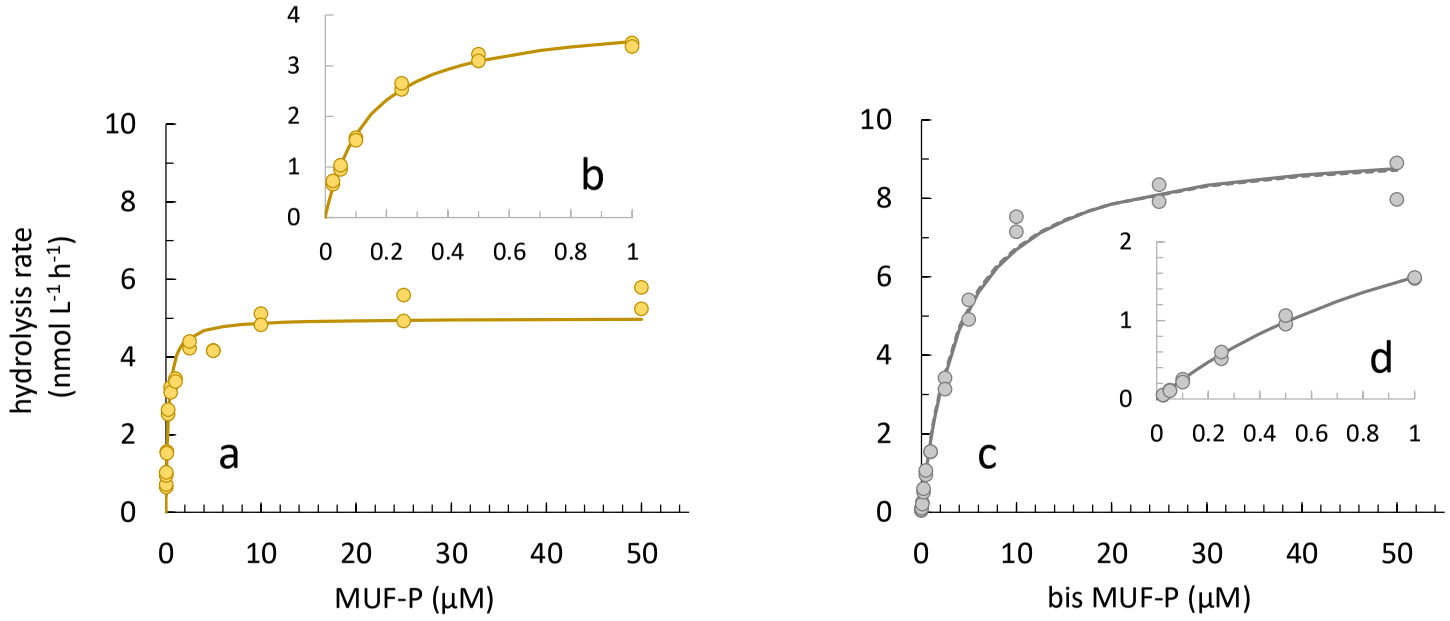

Fig 5

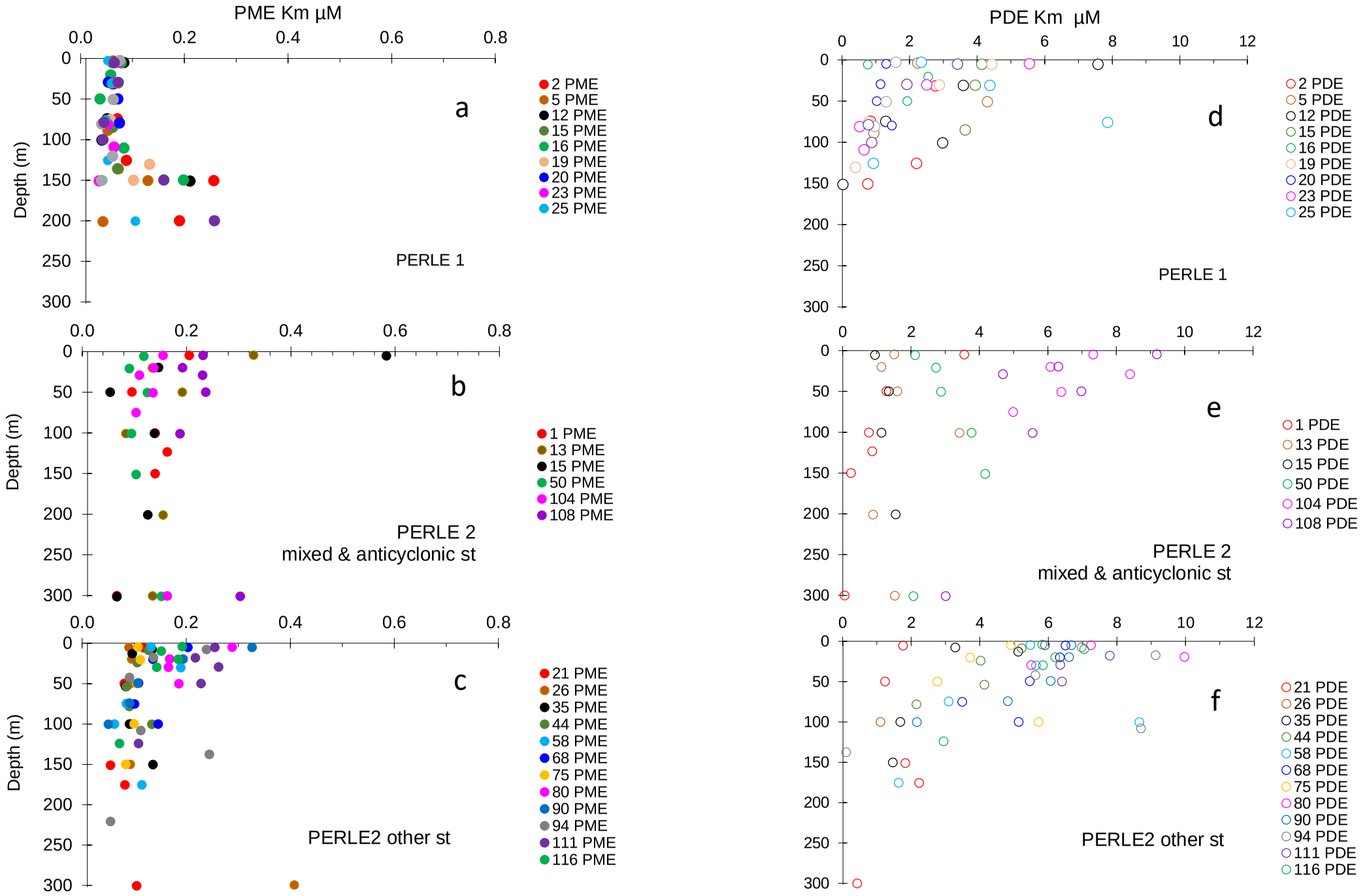
PME Km µM
PDE Km µM
Depth (m)
a
b
c
d
e
f
PERLE 1
PERLE 2
mixed & anticyclonic st
PERLE2 other st
2 PME
5 PME
12 PME
15 PME
16 PME
19 PME
20 PME
23 PME
25 PME
1 PME
13 PME
15 PME
50 PME
104 PME
108 PME
21 PME
26 PME
35 PME
44 PME
58 PME
68 PME
75 PME
80 PME
90 PME
94 PME
111 PME
116 PME
2 PDE
5 PDE
12 PDE
15 PDE
16 PDE
19 PDE
20 PDE
23 PDE
25 PDE
1 PDE
13 PDE
15 PDE
50 PDE
104 PDE
108 PDE
21 PDE
26 PDE
35 PDE
44 PDE
58 PDE
68 PDE
75 PDE
80 PDE
90 PDE
94 PDE
111 PDE
116 PDE

Fig 6

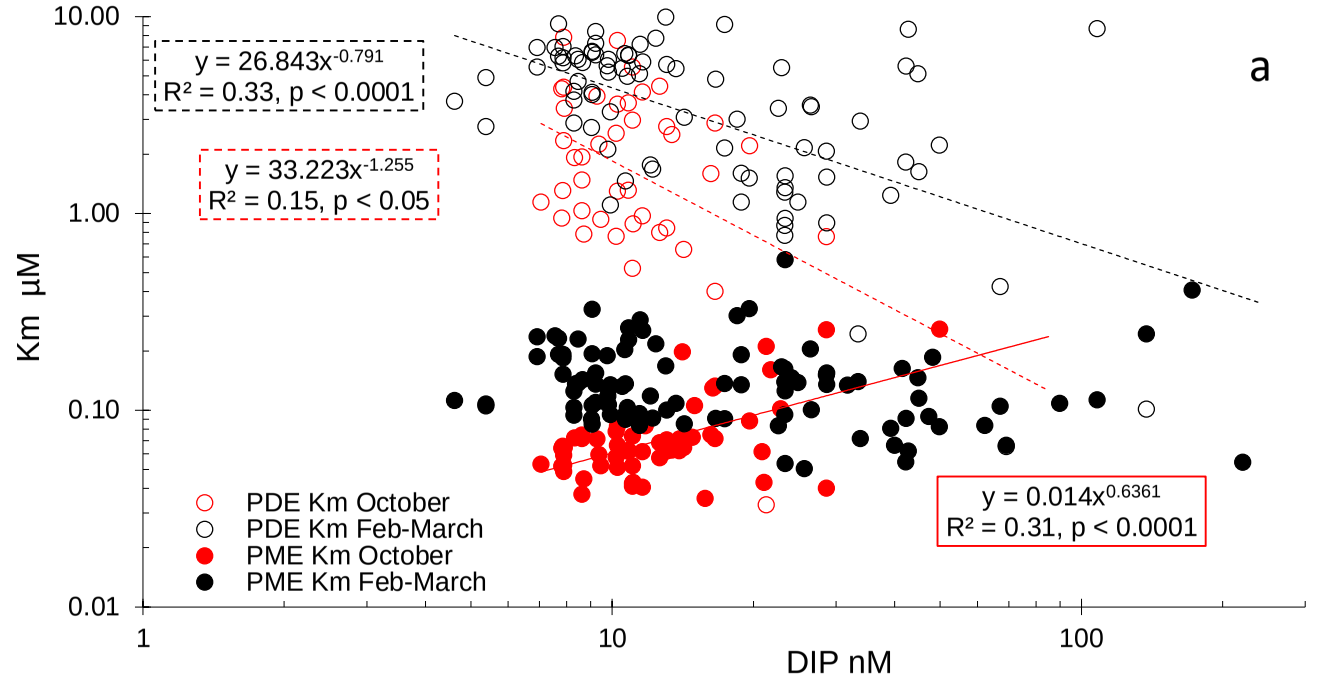
a
y = 26.843x^-0.791
R² = 0.33, p < 0.0001
y = 33.223x^-1.255
R² = 0.15, p < 0.05
y = 0.014x^0.6361
R² = 0.31, p < 0.0001
PDE Km October
PDE Km Feb-March
PME Km October
PME Km Feb-March
Km µM
DIP nM
10.00
1.00
0.10
0.01
1
10
100

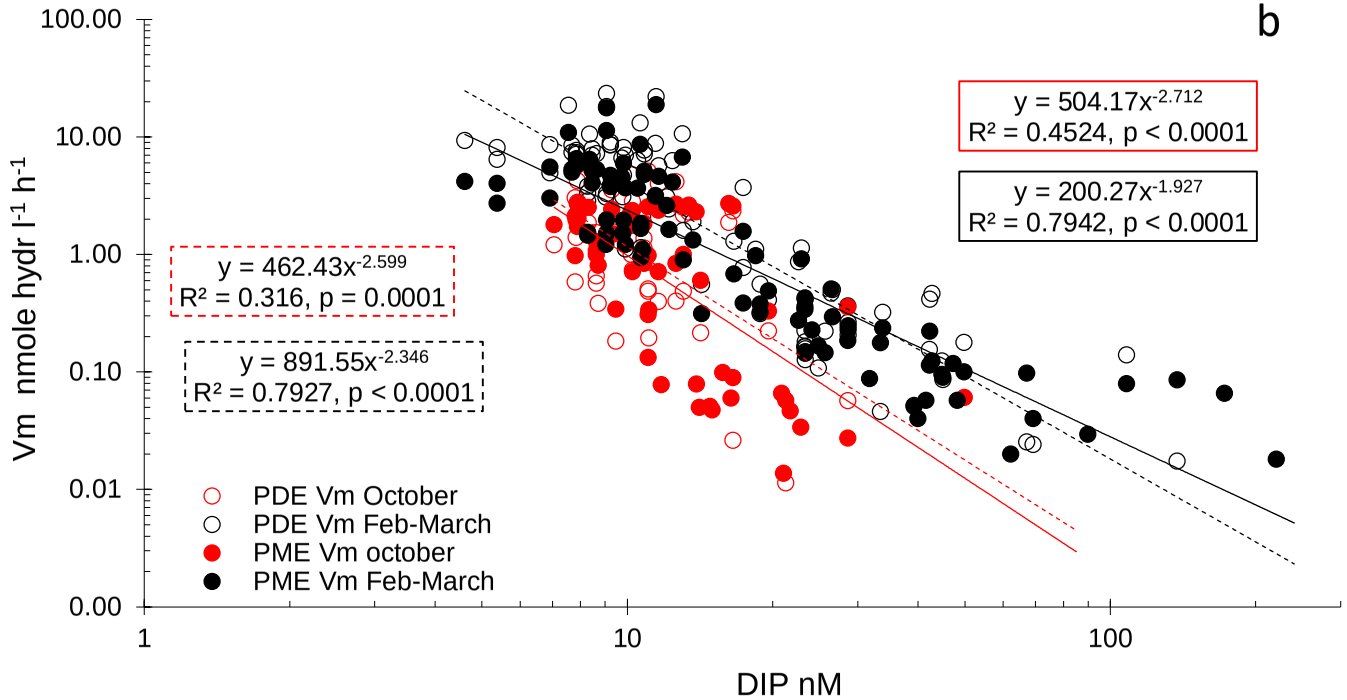
b
y = 504.17x^-2.712
R² = 0.4524, p < 0.0001
y = 200.27x^-1.927
R² = 0.7942, p < 0.0001
y = 462.43x^-2.599
R² = 0.316, p = 0.0001
y = 891.55x^-2.346
R² = 0.7927, p < 0.0001
PDE Vm October
PDE Vm Feb-March
PME Vm october
PME Vm Feb-March
Vm nmole hydr l-1 h-1
DIP nM
100.00
10.00
1.00
0.10
0.01
0.00
1
10
100

Fig. 7